THE JOURNAL OF BIOLOGICAL CHEMISTRY VOL. 292, NO. 2, pp. 611–628, January 13, 2017

Secreted Glioblastoma Nanovesicles Contain Intracellular Signaling Proteins and Active Ras Incorporated in a Farnesylation-dependent Manner*[S]

Received for publication, July 8, 2016, and in revised form, November 11, 2016 Published, JBC Papers in Press, December 1, 2016, DOI 10.1074/jbc.M116.747618

Natalie Luhtala[‡1], **Aaron Aslanian**[‡§2], **John R. Yates III**[§], **and Tony Hunter**[‡3]

From the [‡]*Molecular and Cell Biology Laboratory, Salk Institute for Biological Studies, La Jolla, California 92037 and the* [§]*Department of Chemical Physiology, The Scripps Research Institute, La Jolla, California 92037*

Edited by Alex Toker

Glioblastomas (GBMs) are malignant brain tumors with a median survival of less than 18 months. Redundancy of signaling pathways represented within GBMs contributes to their therapeutic resistance. Exosomes are extracellular nanovesicles released from cells and present in human biofluids that represent a possible biomarker of tumor signaling state that could aid in personalized treatment. Herein, we demonstrate that mouse GBM cell-derived extracellular nanovesicles resembling exosomes from an H-RasV12 myr-Akt mouse model for GBM are enriched for intracellular signaling cascade proteins (GO: 0007242) and Ras protein signal transduction (GO: 0007265), and contain active Ras. Active Ras isolated from human and mouse GBM extracellular nanovesicles lysates using the Ras-binding domain of Raf also coprecipitates with ESCRT (endosomal sorting complex required for transport)-associated exosome proteins Vps4a and Alix. Although we initially hypothesized a role for active Ras protein signaling in exosome biogenesis, we found that GTP binding of K-Ras was dispensable for its packaging within extracellular nanovesicles and for the release of Alix. By contrast, farnesylation of K-Ras was required for its packaging within extracellular nanovesicles, yet expressing a K-Ras farnesylation mutant did not decrease the number of nanovesicles or the amount of Alix protein released per cell. Overall, these results emphasize the primary importance of membrane association in packaging of extracellular nanovesicle factors and indicate that screening nanovesicles within human fluids could provide insight into tissue origin and the wiring of signaling proteins at membranes to predict onset and behavior of cancer and other diseases linked to deregulated membrane signaling states.

Exosomes are tiny (50–150 nm) extracellular vesicles that have been implicated in a number of physiologically relevant processes: prion protein transmission and neurodegenerative diseases (1), regulation of immune functions (2), tumor angiogenesis (3–15), fibroblast signaling to tumors (16, 17), and priming of the metastatic niche (18–25). Recent research indicates that exosomes from bodily fluids such as blood, urine, and cerebrospinal fluid can carry information valuable in diagnostics or treatment of human pathologies (26–31). Overall, increased knowledge of exosome functions could enable us to rationally predict and/or target tumorigenesis.

Ras protein signaling is important for glioblastoma (GBM)[4] tumorigenesis. Mouse tumors initiated through doxycycline-inducible expression of mutant K-Ras in the brain can be reverted by shutting off its expression (32). Activating Ras as a result of genetic mutations to NF1 and p53 or by hippocampal injection of lentiviruses for shRNA targeting of NF1 and p53 is also sufficient to produce human GBM-like tumors in mice (33, 34). Deregulated Ras signaling occurs in certain human GBMs due to functional loss of NF1, a GTPase-activating protein that regulates Ras·GTP and can be inactivated in GBM either proteasomally or genetically (35). Loss of p53 function in human GBMs prevents Ras signaling-induced senescence (36); p53 can be inactivated either genetically or through MDM2-mediated sequestration (37). Thus, combined loss of NF1 and p53 function augments Ras signaling in GBM. In addition, activation of growth factor receptor signaling at GBM cell membranes upstream of Ras increases Ras signaling in GBM (38–41). Corroborating a role for Ras signaling driving human GBM tumors, human GBM cell lines exhibit sensitivity to Ras pathway inhibitors (42–47). Exosomes, which carry Ras proteins (48–50), represent a possible carrier of information about the wiring of Ras or other tumor signals that could be useful in personalizing treatment protocols to better target the tumors of patients.

Here, we examined extracellular nanovesicles (NVs) released from cultured cells established from GBM tumors induced by hippocampal injection of lentiviruses to drive the combined activation of H-Ras and AKT in GFAP-Cre $Tp53^{+/-}$ mice (51).

* This work was supported in part by National Institutes of Health NCI Grants CA194584, CA80100, and CA82683 (to T. H.), Cancer Center Support Grant CA14195 (Waitt Advanced Biophotonics Core), and National Center for Research Resources Grant 5P41RR011823-17 and National Institutes of Health NIGMS Grant 8P41GM103533-17 (to J. R. Y.). The authors declare that they have no conflicts of interest with the contents of this article. The content is solely the responsibility of the authors and does not necessarily represent the official views of the National Institutes of Health.

[S] This article contains supplemental Tables S1–S5.

[1] Supported by the George E. Hewitt Foundation for Medical Research Fellowship and American Cancer Society Fellowship 127795-PF-15-030-01-CSM.

[2] Supported by the Leona M. and Harry B. Helmsley Charitable Trust.

[3] American Cancer Society Professor and Renato Dulbecco Chair in Cancer Biology. To whom correspondence should be addressed: 10010 N. Torrey Pines Rd., La Jolla, CA 92037. Tel.: 858-453-4100; E-mail: hunter@salk.edu.

[4] The abbreviations used are: GBM, glioblastoma; ESCRT, endosomal sorting complex required for transport; MudPIT, multidimensional protein identification technology; RBD, Ras binding domain; MVB, multivesicular body; IPI, international protein identifier; EV, extracellular vesicle; TEM, transmission electron microscopy; Tet, tetracycline; Dox, doxycycline; NTA, nanoparticle tracking analysis; NV, nanovesicle.

These NVs isolates were consistent with exosomes in their protein composition and structure. To understand what types of proteins are represented within the GBM exosome proteome as compared with the cellular proteome, we used multidimensional protein identification technology (MudPIT) mass spectrometry (52) to predict total cellular proteins and compared this profile to that of extracellular NVs released from these cells. Our results revealed that extracellular NVs contained an increase in the relative levels of intracellular signaling cascade proteins (GO: 0007242), in particular, those represented within the gene ontology group of Ras protein signal transduction (GO: 0007265). Moreover, active Ras could be purified from extracellular NVs lysates using the Raf-Ras-binding domain (Raf-RBD), and ESCRT-associated proteins were precipitated in this purification.

We performed assays to test the direct contribution of K-Ras activity to exosome biogenesis in both *cis* and *trans*. Through stable, conditional expression of K-Ras in either wild-type or mutant forms in an isogenic GBM background, we investigated the impact of K-Ras GTP binding and farnesylation upon extracellular release and trafficking of Alix and K-Ras to NVs. Although GTP binding of K-Ras was dispensable for its extracellular release to NVs, farnesylation and hence membrane association was required. These findings were interpreted against prior exosome proteomic datasets and support investigating exosomes from human fluids to understand whether information about tissue origin and activity and important protein-protein interactions relating to signaling pathways might be able to inform diagnostics or therapies for patients with cancer or other diseases yielding deregulated membrane signaling.

Results

GBM Cell Extracellular Nanovesicles Resemble Exosomes in Content and Structure and Contain a Distinct Profile of Proteins—Because prior research supports the use of extracellular vesicles (EVs) as biomarkers of GBM and other cancers and diseases, we asked which types of proteins are compartmentalized and released within EVs from GBM cells as compared with the protein content of whole cells. To simplify the interpretation of our results, we probed cultured 005 cells, a cell line established from a mouse model for GBM induced by hippocampal injection of lentiviruses to drive the combined activation of H-Ras and AKT in GFAP-Cre $Tp53^{+/-}$ mice (51). We hypothesized that proteins regulating signaling within these pathways would be highly represented within EVs from 005 cells. We were most interested in exosomes that are produced from intraluminal vesicles following fusion of multivesicular bodies (MVBs) with the plasma membrane because MVBs arise from the regulated action of endosomal sorting complex required for transport (ESCRT) proteins in a process involving ubiquitin (reviewed in Ref. 53). We expected that the ESCRT-regulated pathway dictating sorting of exosome cargoes to MVBs might involve the activity of signaling cargoes originating from the plasma membrane.

Using established protocols (12, 54), we prepared extracellular NVs to enrich for exosomes using ultracentrifugation and filtration of conditioned medium obtained in parallel from cultured 005 cells and U87MG human GBM cells with the goal of comparing 005 mouse GBM extracellular NVs to U87MG human GBM extracellular NVs, which have been previously characterized (55). Progressive ultracentrifugation of conditioned media was used to remove cells ($300 \times g$), dead cells and cellular debris ($16{,}500 \times g$), followed by 200-nm filtration to remove larger vesicles. The final cleared supernatant was pelleted at $110{,}000 \times g$ to isolate NVs. By transmission electron microscopy analysis (TEM) of fixed NVs, we found that both preparations exhibited vesicles with characteristic cup-shaped morphology reported in previous publications for exosomes (Fig. 1*A*). A heterogeneously sized population of vesicles was observed for 005 and U87MG exosome samples with an average size 62.3 ± 23.8 and 80.1 ± 29.9 nm, respectively.

To determine whether the NVs are representative of exosomes, we utilized immunoblots to compare equal amounts of proteins from the attached cells (cell), cells pelleted from the conditioned media (P300), the larger vesicles and cellular debris (P16.5K), and the final, washed NVs. Consistent with the successful concentration of exosomes using this protocol, extracellular NVs isolated from U87MG and 005 cells displayed characteristic enrichment of the MVB regulatory proteins that serve as exosome markers, Alix and Tsg101 (Fig. 1*B*), as well as depletion of the endoplasmic reticulum marker calnexin. In these semiquantitative analyses, we cannot ensure a linear relationship between the signal intensity and antigen loading for the antibodies used and did not have a clear indicator for loading available at the time experiments were performed. However, 005 cell NV samples resolved in parallel on gels demonstrate similar levels of either an antibody cross-reactive band or degradation product of calnexin (Fig. 1*B*, anti-calnexin). The 005 analysis resolved on separate gels from the same sample in parallel demonstrates a clear enrichment for Alix and Tsg101 in NVs as compared with cell, P300, and P16.5K fractions. For U87MG NVs, samples resolved were probed using dual-color analysis on the Odyssey and clearly indicate the presence of Alix in NVs and the absence of calnexin on the same blot for NVs as compared with the cellular fraction that demonstrates a fragmented anti-Alix signal and single prominent band for anti-calnexin. Tsg101 enrichment is demonstrated for the same sample resolved on a separate gel and blot.

To understand whether extracellular NVs exhibit a specific protein profile compared with whole cells, we used SDS-PAGE to resolve and compare equal amounts of total proteins from attached cells (cells), from the $300 \times g$ pelleted cells (P300) from the conditioned media, and from the final, washed NVs. Resolved gels were stained with either Coomassie Blue (005) or silver stain (U87MG), and the results revealed that migration of protein bands for 005 and U87MG extracellular NVs differed from those observed for whole cell and $300 \times g$ pellet samples (Fig. 1*C*). Overall, the size, morphology, enrichment for MVB regulatory exosome proteins, and distinct profile of proteins demonstrated by extracellular NV preparations suggests that these are enriched for exosomes. For the purpose of simplicity, we will refer to these extracellular NV preparations as exosomes herein, noting that we have not analyzed the site of production of these vesicles, and it is indeed possible that not all of the vesicles are produced through MVB fusion with the plasma membrane and that contaminating proteins might still be present.

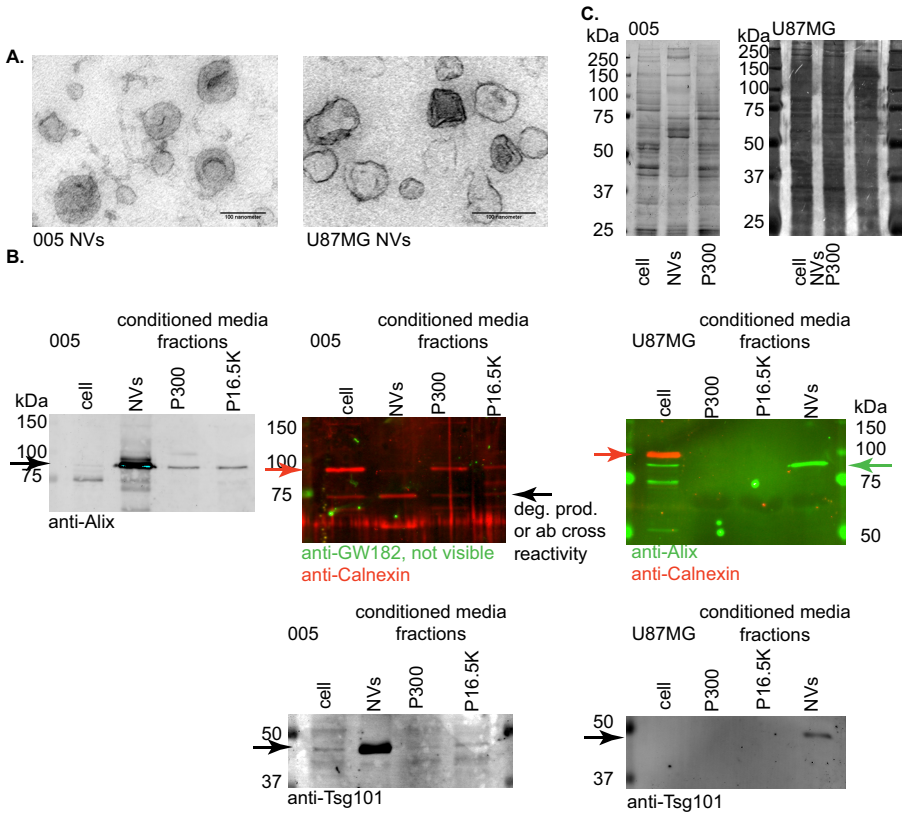

FIGURE 1. **Structure and content of NVs resembles exosomes.** Analysis of fractions for extracellular NVs, attached cells (*cell*), suspended cells (*P300*), and larger vesicles and debris (*P16.5K*) from 005 and U87MG cultured GBM cells. *A*, TEM of fixed NVs. *B*, immunoblots of 10 μg of total proteins for 005 and U87MG NVs probed for the indicated proteins using separate blots for identical samples in parallel or using dual labeling of the same blot on a Li-Cor Odyssey IR scanner. Color-coded *arrows* clarify the positions of the protein of interest. *C*, Coomassie Blue (005) and silver (U87MG) stains of 10 μg of total protein denatured and resolved by SDS-PAGE.

GBM Exosomes Are Significantly Enriched for Intracellular Signaling Cascade and Ras Protein Signal Transduction Proteins—Because we observed a difference in the banding profile of proteins in exosomes as compared with their corresponding whole cells, we sought to identify which specific proteins were included in 005 exosomes as compared with 005 whole cells by performing mass spectrometry analysis of proteins using MudPIT. Equal amounts of total protein from 005 whole cell lysates were compared with 005 exosome sonicates in a non-quantitative analysis to predict proteomes for each based on data observed in all three technical replicates (detailed results, supplemental Table S1). Analyzing proteins predicted in 3 of 3 technical replicates, we recorded 1049 proteins for the identified whole cell proteome and 609 proteins for the identified exosome proteome, with an overlap of 349 proteins, which are represented in a proportional Venn diagram (Fig. 2*A*). Using the Functional Enrichment analysis tool FunRich (56), we recorded that 94% of the identified 005 exosome proteome overlapped with known exosome proteins at ExoCarta exosomes database (57–60) (Fig. 2*B*). To understand the functional differences in identified whole cell and identified exosome proteomes, we used this tool and performed a gene ontology analysis (using GO_BP_FAT generated through Database for Annotation, Visualization and Integrated Discovery (DAVID) version 6.7 functional annotation tool (61, 62)) to identify biological processes significantly ($p = 0.05$ or less) represented by proteins in whole cells *versus* exosomes. A doughnut chart represents a biological process comparison of the 2 datasets using FunRich (Fig. 2*C*), and a complete list of significant and non-significant results for gene ontology biological process analysis by DAVID is available (supplemental Table S2, "GO_BP_FAT_CELL3" and "GO_BP_FAT_EXO3", all terms above the underline are p value less than 0.05).

Interestingly, both DAVID and FunRich annotation tools revealed an enrichment of signal transduction biological processes for the 005 exosome proteomic datasets. A doughnut chart generated by FunRich for biological process comparison of the 005 exosomal proteome to the 005 cellular proteome shows that the greatest percentage of the 005 exosomal proteome is linked to signal transduction processes (29.9%), whereas metabolism accounts for the greatest percentage of the 005 cellular proteome (24%) (Fig. 2*C*, p values and gene details in supplemental Table S3). Using DAVID, we found that small GTPase signal transduction (GO: 0007264) was much more significantly represented in the identified 005 exosome proteome than the identified whole cell proteome, with a p value of 2.32×10^{-18}, whereas its p value was 7.10×10^{-3} for the identified whole cell proteome (supplemental Table S2, "top 10" compare *bold green* type p value to *bold red* type p value). A comparison of the top 10 significantly represented GO biological processes for each proteome, whole cell and exosome, demonstrated that small GTPase signal transduction was the second most significantly represented term for the identified exosome proteome but did not make the top 10 for the identi-

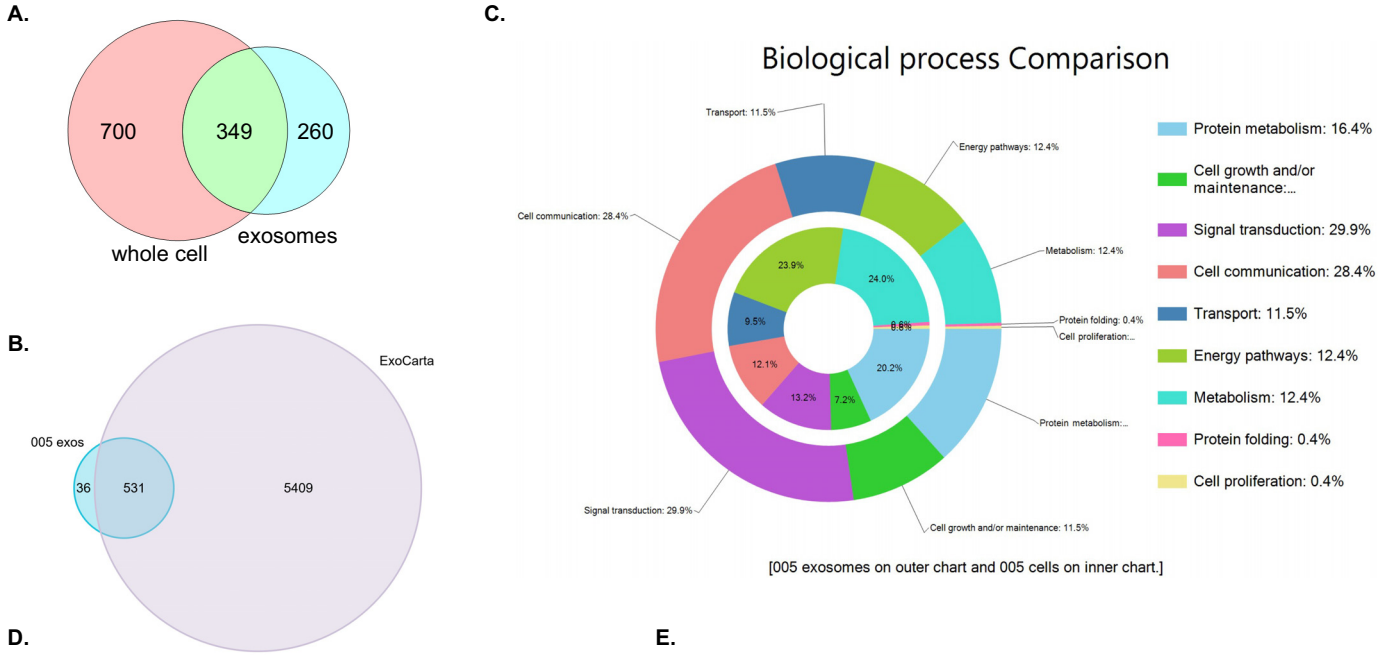

D.

Most significant terms for those only significant for exosomes		
Term	**Description**	**PValue**
GO:0007242	intracellular signaling cascade	2.82E-08
GO:0032989	cellular component morphogenesis	3.91E-08
GO:0000902	cell morphogenesis	6.66E-07
GO:0007155	cell adhesion	1.92E-06
GO:0022610	biological adhesion	1.99E-06
GO:0030031	cell projection assembly	6.03E-06
GO:0030030	cell projection organization	1.09E-05
GO:0007265	Ras protein signal transduction	3.99E-05
GO:0007163	establishment or maintenance of cell polarity	8.82E-05
GO:0000904	cell morphogenesis involved in differentiation	2.17E-04

E.

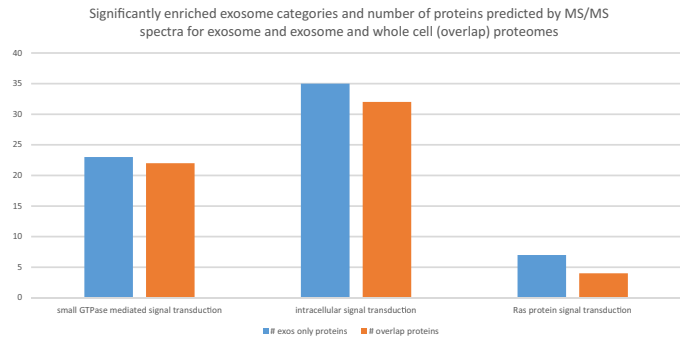

FIGURE 2. **GBM exosomes are enriched for signaling proteins.** MudPIT comparison of equal amounts of proteins for 005 exosomes sonicates and 005 whole cell lysates. *A* and *B,* proportional Venn diagram for (*A*) number of proteins predicted by MS/MS spectra in all 3 technical replicates and (*B*) map able gene symbols for the 005 exosomes dataset compared with ExoCarta exosomes database of proteomes predicted by MS (human, mouse, and rat) using FunRich. *C,* biological process comparison of 005 cells gene symbols to 005 exosomes using FunRich. Gene details and *p* values at supplemental Table S3. *D,* top 10 terms by significance for those with a *p* value of 0.05 or less for exosome but not the whole cell proteome. Overlap with the list in Fig. 3*C* is indicated in *turquoise* type. *E,* number of proteins mapping to GO signaling categories significantly enriched in exosomes.

fied whole cell proteome (supplemental Table S2, top 10). In contrast, translation (GO: 0006412), hexose catabolic process (GO: 0019320), and glucose catabolic process (GO: 0006007) were in the top 10 by significance for both the identified whole cell proteome and identified exosome proteome lists (supplemental Table S2, top 10, *bold black* type).

We wondered whether any significantly represented GO biological process terms would be unique to the identified exosome proteome, because certain proteins were only predicted for the identified exosome proteome, and fewer proteins were identified for exosomes than for whole cells, which would also enhance the significance of the identified terms. Indeed, results from this analysis revealed biological processes significant only for the identified exosome proteome, entailing processes such as signal transduction, adhesion, and morphogenesis (supplemental Table S2, "EXO3_ONLY," and Fig. 2*D*). Specifically, the most significant term represented only in the identified exosome proteome was intracellular signaling cascade (GO: 0007242), and Ras protein signal transduction (GO: 0007265) was the 8th most significant term (Fig. 2*D*), consistent with 005 cells expressing a mutant activated H-Ras protein.

Unique significance for the identified exosome proteome in these categories could simply be due to the smaller number of proteins identified (609 as compared with 1049 in the identified whole cell proteome) or arise also from identification of proteins only in exosomes that regulate these functions. To answer this question, we separately probed for set differences and intersections between the exosome protein ID dataset of a given significantly represented GO biological process (small GTPase signal transduction, intracellular signaling cascade, and Ras protein signal transduction) and compared with the entire set of protein IDs from the filtered list for the identified whole cell proteome. This comparison revealed that although a portion (40–50%) of the proteins were identified in both exosomes and whole cell proteomes, more than 50% of the proteins were exclusively identified in the exosome analysis (Fig. 2*E*). Nevertheless, the "unique" exosome proteins must have been expressed in cells they were derived from, and presumably

their presence in whole cell samples analyzed was below the threshold of detection.

Cytoplasmically Localized Intracellular Signaling Proteins Maintain Their Topology and Are Vesicularly Associated—Our mass spectrometry analysis predicted a significant representation of signaling proteins and translation proteins in the identified exosome proteome. We were interested in the potential for intercellular exchange of signaling and translation-associated proteins via exosomes, and we wondered whether the proteins that we identified were indeed in their native, functional state within vesicles. Alternatively, these could represent proteins on the surface of exosomes, either due to interactions of proteins from permeabilized cells with exosome membranes (artifactual) or due to physiological relocalization of cytoplasmic proteins to the cell surface. Cytoplasmic signaling proteins maintaining their normal, cellular, topology should be protected from added protease (trypsin) degradation by the exosome membrane (which can be disrupted by a detergent such as Triton X-100), and this effect should be similar to that observed for a soluble, cytoplasmic exosome protein such as Alix. To verify that a free, non-vesicular protein can be digested by trypsin alone, we spiked in purified GST-Ubc9 and analyzed its degradation profile as well.

We found that cytoplasmic signaling proteins Ras and β-catenin in both 005 and U87MG exosomes were protected from digestion by trypsin alone, similarly to Alix, yet disrupting the exosome membrane with detergent was sufficient to enable trypsin digestion of all of these proteins (Fig. 3*A*, compare anti-Ras and anti-β-catenin to anti-Alix). Tsg101, detectable in 005 exosomes but not U87MG exosomes in this experiment, yielded a similar profile to that of Alix (Fig. 3*A*, *anti-Tsg101*). In contrast, GST-Ubc9 could be readily digested by trypsin alone, demonstrating that as expected free soluble proteins in the exosome preparation are sensitive to trypsin in the absence of detergent (Fig. 3*A*, *anti-GST*). Interestingly, very little of the Rps3 ribosomal protein was protected from degradation by trypsin alone in 005 and U87MG exosomes (Fig. 3*A*, *anti-Rps3*). Particularly in 005 exosomes, the majority of Rps3 ribosomal protein was not protected from digestion by trypsin alone, *i.e.* Rps3 is a contaminant presumably bound to the exterior of exosomes.

Sucrose cushions can be used to separate proteins nonspecifically associated externally with exosome membranes, and large protein aggregates, which might contaminate exosome preparations made by ultracentrifugation. Because a sucrose cushion step was not used in the preparation of 005 exosomes for mass spectrometry, we performed this step to examine retention of Ras, β-catenin, and Rps3 in exosomes prepared by our original ultracentrifugation protocol followed by purification on a sucrose cushion. In addition, we examined histone H3, a protein we observed abundantly in 005 exosomes that we predicted could be an artifactual contaminant in these preparations. For comparison, we looked at the percent retention of Alix and the percentage retention of the integrin α5, a protein that associates with β1 integrin to act as a fibronectin receptor and has been demonstrated to sort to multivesicular bodies in a ubiquitin-dependent manner and complex with Tsg101, an ESCRT-I protein (63).

Exosomes were diluted in PBS and pelleted onto a 30% D_2O sucrose cushion (54). Importantly, β-catenin and Ras were both retained on the cushion at a percentage equivalent to that of Alix (Fig. 3*B*, 5.4 and 4.4%, respectively, as compared with 4.2% for Alix). Integrin α5, an integral membrane protein and substrate for ESCRT, was retained at an even greater percentage (Fig. 3*B*, 5.7%). In contrast, Rps3 was retained only at 1.6%, consistent with the trypsin digestion data demonstrating that only a small portion of Rps3 was inside vesicles (Fig. 3*B*, *bottom panel*), and histone H3 was retained at an even lower percentage (Fig. 3*B*, 0.4%). Moreover, the PBS solution above the sucrose cushion contained trace amounts of all proteins except Rps3 and histone H3 (Fig. 3*B*, *top layer*), indicating that Rps3 and histone H3 are not truly vesicularly associated and cannot float on the sucrose cushion.

To understand whether cushion isolation of exosomes would alter which proteins are enriched in exosomes as compared with whole cells, we prepared exosomes from 005 cells by this method. In this analysis, we compared exosomes to whole cell sonicates to probe the contribution of the lysis buffer to the comparison such that equal amounts of total protein were compared between 005 sucrose cushion-isolated sonicates and whole cell sonicates. In this MudPIT analysis, slightly fewer proteins were predicted for each proteome than in the first analysis (878 for whole cell and 431 for exosomes, with 202 overlapped proteins, compared with 1049 and 609, with 349 overlapped proteins, see supplemental Table S4). This analysis was primarily non-quantitative, but NSAF values are available (supplemental Table S4, *NSAF tab*), which can approximate amounts of proteins for comparison (64). Nearly 70% (296) of the 431 proteins from sucrose cushion exosomes overlapped with proteins predicted by the first mass spectrometry analysis, whereas over 75% (663) of the 878 proteins predicted for whole cell sonicates demonstrated overlap with the first experiment using whole cell lysates. Gene ontology GO_BP_FAT charts were again generated using DAVID for identified whole cell and identified exosome proteomes separately, and these were compared with defined biological process categories unique to either whole cells or exosomes proteomes. Significant and non-significant results of this comparison are available (supplemental Table S5). The top 10 terms significantly represented by the identified exosome proteome, but not the identified whole cell proteome, were defined, and these resembled that of the first analysis for 5 of the 10 terms (overlap noted in *turquoise* type, compare Fig. 2*D* to Fig. 3*C*).

Interestingly, small GTPase signal transduction (GO: 0007264) was now the most significantly represented biological process for 005 exosomes, and this term was no longer significant for the identified whole cell proteome (supplemental Table S5). In contrast, *p* value changes demonstrate that translation (GO: 0006412) was now less significantly represented in the identified exosome proteome (3.5×10^{-5}) than in the analysis of less purified exosomes (6.0×10^{-23}). However, this term was more significantly represented based on the *p* value in this analysis (6.4×10^{-43}) for the identified whole cell proteome than in the previous analysis (4.1×10^{-42}). Moreover, the significance of intracellular signaling cascade (GO: 0007242) and Ras protein signal transduction (GO: 0007265) terms improved in this anal-

ysis as well (compare Fig. 2*D* to Fig. 3*C*). FunRich comparisons of the sucrose cushion-purified exosomes (005 SC exosomes) data to Fig. 2*A* proteomic data for 005 exosomes (without sucrose cushion) revealed increased representation for cellular components with membranes such as exosomes and the plasma membrane (Fig. 3*D*, supplemental Table S3). Moreover, sucrose cushion-purified exosomes retained a greater percentage of signal transduction proteins (Fig. 3*E*, supplemental Table S3). In contrast, proteins linked to the ribosome were reduced in this dataset, consistent with data showing a decreased significance for translation in this dataset and Rps3 degradation by trypsin (Fig. 3, *A*, *B*, and *D*, supplemental Table S3). Thus, sig-

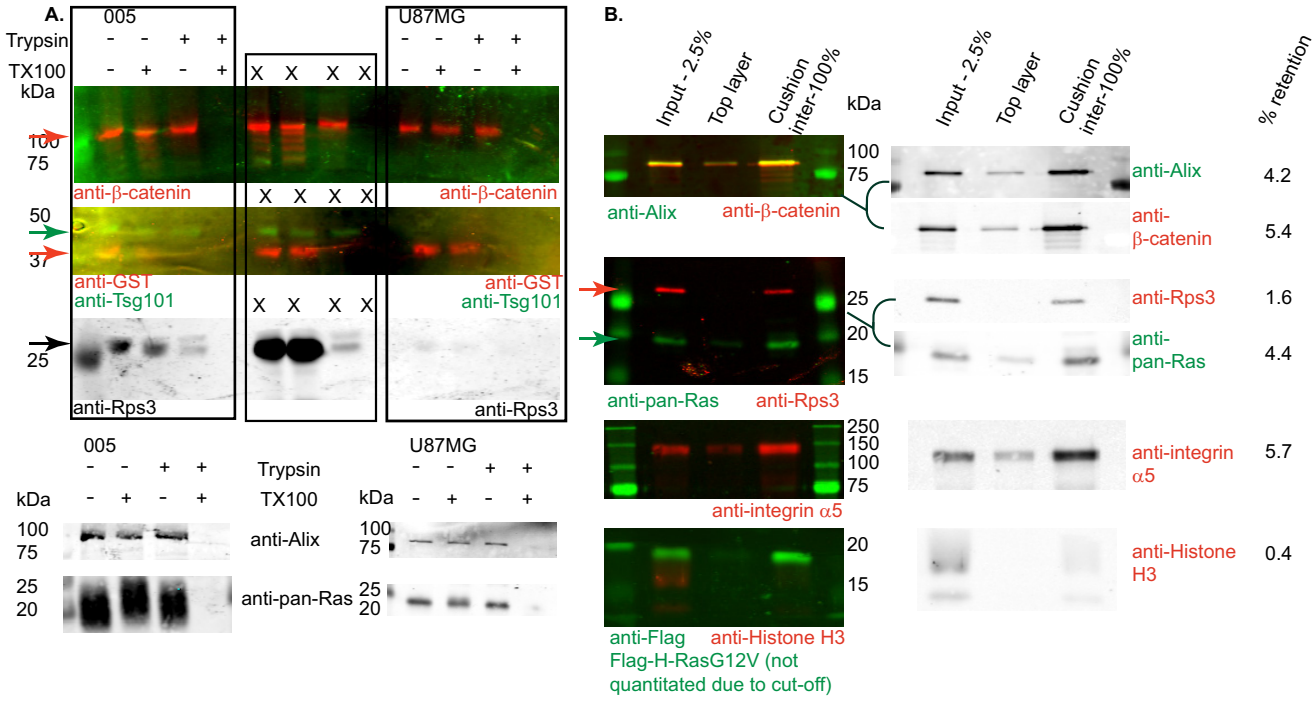

C.

Most significant terms for those only significant for exosomes (cushion)		
Term	**Description**	**Pvalue**
GO:0007264	small GTPase mediated signal transduction	3.5E-22
GO:0007242	intracellular signaling cascade	9.42E-14
GO:0016192	vesicle-mediated transport	1.29E-11
GO:0007265	Ras protein signal transduction	1.45E-07
GO:0006897	endocytosis	7.48E-07
GO:0010324	membrane invagination	7.48E-07
GO:0016044	membrane organization	1.1E-05
GO:0032989	cellular component morphogenesis	1.6E-05
GO:0000902	cell morphogenesis	6.83E-05
GO:0007155	cell adhesion	0.000108

D.

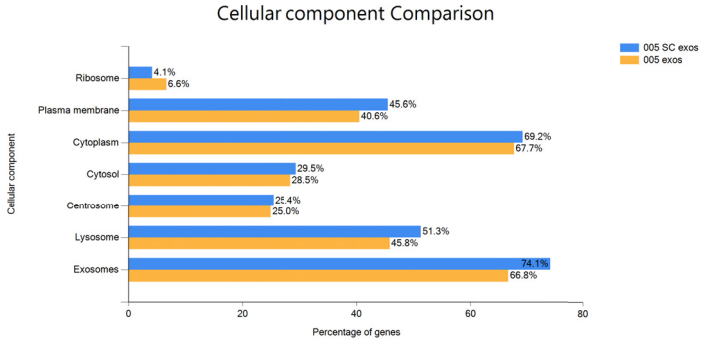

E.

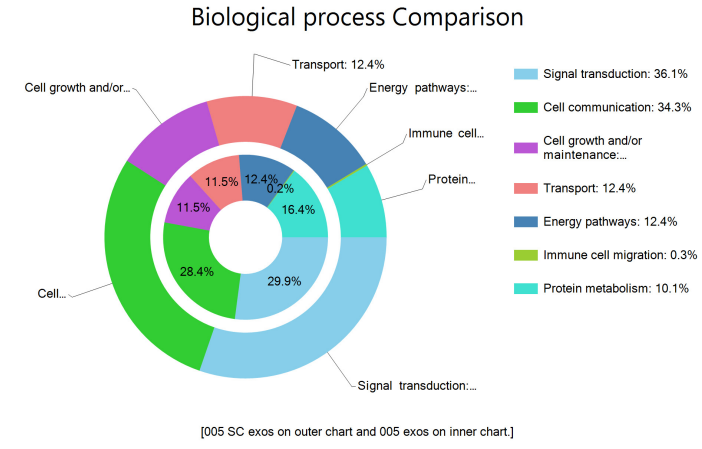

[005 SC exos on outer chart and 005 exos on inner chart.]

naling proteins, but not translation machinery proteins, are specifically enriched in exosomes.

Active Ras and ESCRT-associated Proteins Specifically Copurify with the Raf Ras-binding Domain from GBM Exosomes Lysates—Because exosomes carry an abundance of signaling proteins, we wondered whether these proteins would be wired to transmit an active signal to cells taking up exosomes. In particular, we expected that active Ras (bound to GTP) should be found in exosome lysates if exosomes were indeed able to manipulate the Ras signaling pathway of cells taking up these vesicles. Moreover, we thought that active Ras might complex with protein regulators that could account for its packaging within exosomes.

To test these hypotheses, we used an active Ras detection kit (Cell Signaling), which uses the purified GST-Raf-RBD fusion to selectively bind to GTP-bound Ras (65). Complexed proteins are then affinity precipitated using glutathione resin, and eluted, and subsequently analyzed by SDS-PAGE and immunoblotting to determine whether active Ras and other proteins are precipitated by interaction with the RBD. For these analyses, we used exosomes purified by ultracentrifugation from conditioned medium of 005 cells and U87MG cells to test whether active Ras is packaged in exosomes from cells driven by H-RasV12 constitutive signaling (005) and also in exosomes from human GBM cells devoid of Ras mutations but sensitive to Ras pathway inhibitors (U87MG) (44, 66). Eluates from the GST-Raf-RBD resin were resolved alongside reserved input, unbound, and wash fractions by SDS-PAGE, and we immunoblotted for pan-Ras signals. In parallel, we immunoblotted for exosome regulators: Vps4a, an ESCRT-interactor demonstrated previously to interact with H-Ras, and Alix, another ESCRT-interactor. In addition, we probed for integrin α5 because it represents an ESCRT interactor and MVB substrate, which is abundant in exosomes prepared from both 005 and U87MG lines (63). Immunoblots were scanned, and the percentage retention (percent of the final eluate of the proteins signal as compared with the input of the proteins signal) was calculated for comparisons as a percentage of the GST-Raf-RBD retained for each sample.

Our results demonstrated that Ras proteins were retained at 77 and 64% of the amount of GST-Raf-RBD retained in 005 and U87MG exosomes, respectively, demonstrating that both mouse and human GBM exosomes contain similar amounts of Ras in an active GTP-bound state (Fig. 4, compare top 2 panels). Traces of signal can be observed for the pan-Ras signal in the unbound fraction for both 005 and U87MG exosomes, suggesting that some of the Ras in exosomes was not GTP bound, inactivated either during cell culture or artifactually during the exosome preparation process. Nevertheless, we conclude that GBM exosomes do contain active Ras proteins.

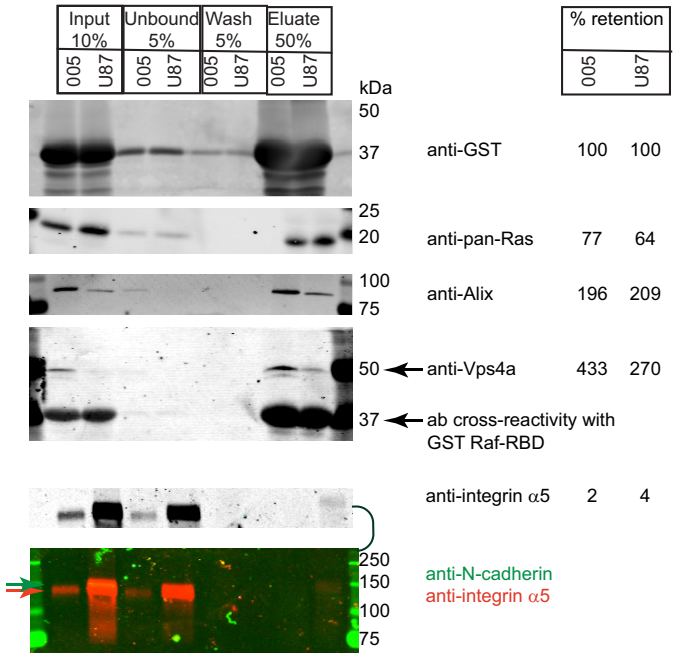

FIGURE 4. **Active exosomal Ras specifically copurifies with ESCRT-associated proteins in Raf-RBD affinity purifications.** Active Ras was affinity purified from 005 and U87MG exosomes lysates using GST-Raf-RBD and glutathione resin, and fractions were resolved by SDS-PAGE and probed with the indicated antibodies. *Top 3 panels* are from one gel; *fourth* and *fifth panels* are from another gel. Gels were cut to transfer separately for blotting with multiple antibodies. Fraction retention was calculated using a signal for eluate divided by signal for input (multiplied by 5 to normalize to 50% eluate loaded). This fraction was divided by the fraction retention for GST-Raf-RBD samples, and multiplied by 100 to give %. Li-Cor Odyssey IR dual color image, *color-coded arrows* clarify the positions of the protein of interest. Cross-reactive band on the anti-Vps4a blot indicates the signal for GST-Raf-RBD.

Regulators of exosome biogenesis and ESCRT were also precipitated by GST-Raf-RBD. The Alix protein was retained at twice the level of GST-Raf-RBD for 005 and U87MG exosomes, and Vps4a was retained at even greater percentages of 433 and 270% (Fig. 4, 3rd and 4th panels). However, integrin α5, which interacts with the ESCRT complex, was very poorly retained (2 and 4% for 005 and U87MG exosomes, respectively) and highly abundant in the unbound fraction (Fig. 4, bottom 2 panels). N-cadherin, a focal adhesion protein probed on the same blot (Fig. 4, anti-N-cadherin, *green arrow*, *yellow band* in U87MG input lane), did not co-precipitate with active Ras either although these data were not quantitated because detection of N-cadherin in exosomes was observed for U87MG but not 005 exosomes samples. These results suggest that Ras proteins are complexed specifically with ESCRT regulators within exosomes

FIGURE 3. **Cytoplasmic signaling proteins localize inside of vesicles.** *A,* immunoblots of equal amounts of exosome preps treated to trypsin protection assays as described. The *top 3 panels* originated from the same gel cut to the blot using multiple antibodies. Others are from separate gels resolved from the same samples in parallel. An irrelevant set of samples are included to avoid splicing the gel and are indicated by "X" *above the lanes*. *B,* SDS-PAGE of 005 exosomes isolated on a sucrose cushion. Analysis of the following: 25 mg of total exosome protein for input (2.5%), pelleting of the top PBS layer above the cushion, and the cushion/PBS interface containing highly purified vesicles for MS analysis. % retention was calculated using the signal for cushion interface divided by the input signal (multiplied by 40 to account for 100% loaded of cushion) and multiplied by 100 to give a %. To conserve sample for multiple antibody probing, *top 2 panels* represent one gel cut and *bottom 2 panels* represent a separate gel run using the same samples in parallel and also cut. *A* and *B,* Li-Cor Odyssey IR dual color images, *color-coded arrows* clarify the positions of the protein of interest. *C,* top 10 terms by significance for those with a *p* value of 0.05 or less for exosome cushion proteome but not the whole cell proteome. Overlap with the list in Fig. 2*D* is indicated in *turquoise* type. *D* and *E,* comparisons of 005 exos (Fig. 2*A*) to sucrose cushion purified (005 SC exos) using FunRich. Gene details and *p* values are in supplemental Table S3.

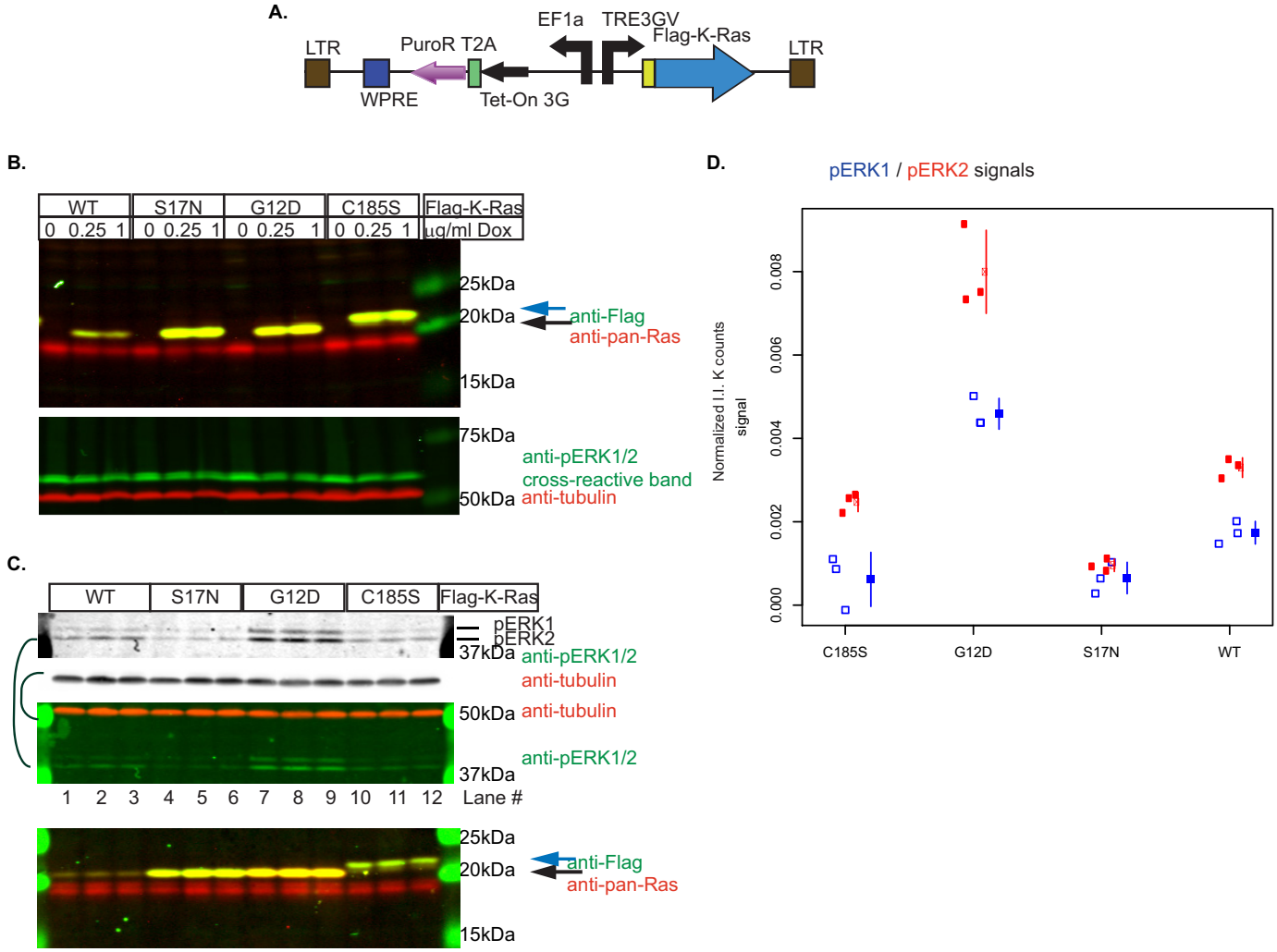

FIGURE 5. **Validation of U87MG cells stably expressing Tet-Flag-K-Ras.** U87MG cells stably expressing Tet-Flag-K-Ras (*A*) as indicated were seeded onto 6-well plates and induced with the indicated concentration of Dox (*B*) or 0.25 μg/ml of Dox (*C*). *B* and *C*, immunoblots for the indicated antibodies comparing lysates prepared from cells growing in wells 48 h after induction. *Green font* and *red font* correspond to signals in 700 and 800 nm channels of Li-Cor Odyssey, respectively, and indicate the relative position of the protein of interest. *Blue arrows* mark the position of unfarnesylated Flag-K-Ras, *black arrows* indicate farnesylated Flag-K-Ras. *B* and *C*, each is a single gel cut to probe as 2 immunoblots. *D*, immunoblot from *C*, signal normalized to tubulin and averaged for 3 independent lysates, plotted as *open blue squares* for pERK1, and *filled red squares* for pERK2, with mean represented by *symbols* and segments to depict mean ± S.D.

and that precipitation by the GST-Raf-RBD is due to their interactions with Ras (perhaps via Vps4a) but not the RBD. This would be consistent with a prior publication demonstrating a role for Vps4a and CHMP6, ESCRT-III interactors, in mediating the recycling of Ras proteins to the plasma membrane (67).

Conditional Expression of K-Ras WT and Mutant Forms in GBM Cells Produces Expected Phenotypes—The proteome of GBM exosomes is enriched for intracellular and Ras signaling proteins and contains active Ras in a functional orientation. We wondered whether active Ras signaling might contribute in *cis* to its exosomal packaging or might regulate the trafficking of other factors to exosomes in *trans*. To address this question, we analyzed exosomes and their corresponding U87MG cells expressing wild-type Flag-K-Ras or mutants of K-Ras altered for K-Ras signaling.

We included mutants in our studies to examine two primary processes required for active Ras signaling: C-terminal farnesylation and GTP binding. First, we focused on the K-Ras G12D mutant, not only due to its oncogenic impact, but also due to its reduced capacity for GTP hydrolysis and existence in a predominantly GTP-bound state (68). Second, we used the K-Ras S17N dominant-negative mutant for analysis, because it is membrane localized (69) but demonstrates a reduced affinity to bind GTP (70). Third, we examined the K-Ras C185S mutant, disrupted for farnesylation at the C-terminal CAAX sequence and thus membrane-delocalized yet capable of binding GTP (69).

To examine exosome biogenesis in U87MG cells stably expressing K-Ras WT or mutants individually in otherwise isogenic strains, we created a single lentiviral vector to conditionally express Flag-K-Ras through a third generation tetracycline (Tet)-responsive system (Fig. 5*A*). After stable integration and puromycin selection, we validated the ability of this system to express K-Ras forms, examining cellular expression using two different concentrations of the more stable Tet analogue doxycycline (Dox) for induction. The results demonstrated repression of expression in the absence of Dox, but both Dox

concentrations yielded similar levels of expression (Fig. 5*B*). Consequently, we selected the lower concentration (0.25 μg/ml of Dox) for induction in subsequent studies.

Because these mutants of K-Ras have not been expressed in U87MG cells in prior publications, we performed assays to validate the U87MG cell response to expression of K-Ras mutants as compared with wild-type K-Ras. Lack of farnesylation in the C185S K-Ras was clearly evidenced by its reduced electrophoretic mobility compared with WT, S17N, and G12D K-Ras (Fig. 5, *B* and *C*, compare *blue arrow* to *black arrow*). To understand the functional impact of C185S and other mutations, we examined phosphorylation of ERK1 and ERK2 (pERK1/2) at Thr-202/Tyr-204 (71) as compared with WT, performing this experiment on triplicate samples. We followed an identical protocol to that used for Fig. 5*B*, but in this instance, we used only 0.25 μg/ml of Dox for induction.

The results clearly show that altering the GTP binding state or membrane association of K-Ras affected downstream phosphorylation of ERK1 and ERK2. First, increasing the activity of K-Ras by reducing GTPase activity as in the G12D mutant led to an increase in the amount of pERK1 and pERK2 observed (compare Fig. 5*C, lanes 7–9* to *1–3*), calculated on average to be roughly 2.5-fold of WT for both pERK1 and pERK2 (Fig. 5*D*). Second, consistent with previously reported dominant-negative effects of the GTP-binding mutant S17N (70), we found that S17N expression reduced pERK1 and pERK2 phosphorylation (compare Fig. 5*C, lanes 4–6* to *1–3*), yielding a >60 and 70% decrease on average (Fig. 5*D*). Third, interfering with the farnesylation and membrane association in the C185S mutant was sufficient to decrease the phosphorylation of pERK1 from WT (top band, compare Fig. 5*C, lanes 10–12* to *1–3*). These effects were similar to the S17N mutant (top band, compare Fig. 5*C, lanes 10–12* to *4–6*) and demonstrated that the signal was 0.4-fold that of WT on average for pERK1 (Fig. 5*D*). In addition, a modest reduction (0.8-fold of WT on average, Fig. 5*D*) in pERK2 levels was also observed by comparing C185S expression to that of WT (Fig. 5*C*, compare *bottom band* in *lanes 10–12* to *lanes 1–3*).

K-Ras Farnesylation, but Not GTP Binding Activity, Is Required for K-Ras Packaging within Exosomes—To assess whether the ability of K-Ras to signal actively would affect K-Ras packaging and secretion in exosomes, we prepared whole cell lysates and exosomes from U87MG cells stably expressing WT, G12D, S17N, or C185S Flag-K-Ras. Cell-normalized equivalents of exosomes and cell lysates were immunoblotted with anti-FLAG signal antibodies to detect Flag-K-Ras forms and pan-Ras antibodies to determine the fraction of Flag-K-Ras expressed within cells and trafficked to exosomes. We normalized the signals to integrin α5, because this protein was abundantly expressed in GBM exosomes but failed to coprecipitate with Ras and Alix in affinity pulldowns of active Ras (Fig. 4), indicating that trafficking of integrin α5 to GBM exosomes is independent of Ras protein signaling. Because Alix coprecipitated with Ras proteins in the affinity precipitation experiment (Fig. 4), we examined the levels of Alix to learn whether modulating Ras signaling might specifically alter the amount of Alix trafficked to exosomes or change the total amount of exosomes released per cell. We also included a similar analysis for the 16,500 $\times$ *g* pellets of larger vesicles and cellular debris (P16.5K) in case these samples revealed a largely different phenotype than that of exosomes.

We found that Flag-K-Ras C185S, which cannot be farnesylated, failed to traffic to exosomes. In three independent experiments, we did not observe any signal for Flag-K-Ras C185S in exosomes, even though it was clearly expressed in cells at levels similar or greater than Flag-K-Ras WT (Fig. 6*A*, *blue arrow*). Furthermore, a signal for endogenous Ras proteins was evidenced in exosomes and cells at similar levels to samples for cells expressing Flag-K-Ras WT, S17N, or G12D (compare *blue arrow* anti-FLAG signal to *black arrow* anti-pan-Ras signal in Fig. 6*A*). Quantitative analysis of three independent experiments demonstrated that Flag-K-Ras C185S was poorly expressed on average as a fraction of total Ras in exosomes as compared with Flag-K-Ras WT (Fig. 6*B*, *red open squares*), whereas cellular expression was greater on average for Flag-K-Ras-C185S as compared with Flag-K-Ras WT using fraction of total Ras as a metric (Fig. 6*B*, *blue filled squares*).

By contrast, both the S17N and G12D mutants of Flag-K-Ras were more highly expressed in exosomes than WT (Fig. 6*A*) when comparing their signals as a fraction of total Ras (Fig. 6*B*, compare *red filled square* data points among WT, S17N, and G12D). In this case, however, the greater fraction of total Ras expression for Flag-K-Ras mutants S17N and G12D as compared with WT can be primarily attributed to a difference in the cellular expression of the mutants (compare *blue open square* data points in Fig. 6*B*). Thus, the S17N and G12D mutants of Flag-K-Ras are trafficked to exosomes to similar extents, indicating that the ability to bind GTP with high affinity does not significantly impact the targeting of Flag-K-Ras to exosomes.

As for the larger vesicles of the P16.5K samples, which were loaded at slightly less (3-fold) cell equivalents than exosomes, we were able to detect Flag-K-Ras S17N in these samples more so than that of other K-Ras forms (Fig. 6*A*, *cutout*). The C185S form of Flag-K-Ras was also not apparent although Flag-K-Ras WT expression was difficult to detect as well. Nevertheless, S17N did not block release of K-Ras to larger vesicles, so we decided against further analysis of these larger vesicles.

Because we had wondered whether altering Ras signaling by expressing K-Ras mutants could also change either total amounts of exosomes released per cell or the specific trafficking of Alix exosome protein to exosomes, we examined both the amount of Alix present in cell-normalized equivalents as a fraction of total Ras in exosomes and the total number of vesicles per cell predicted by NanoSight NTA (nanoparticle tracking analysis) technology for the panel of cells stably expressing Flag-K-Ras WT and mutants. Our initial results demonstrated that the amount of Alix trafficked to exosomes as a fraction of total Ras was not significantly different in samples from cells expressing the WT or mutants of Flag-K-Ras (Fig. 6*A*, *anti-Alix*, *anti-pan-Ras*). Furthermore, averaging three independent experiments demonstrated that similar amounts of Alix were present in exosomes from WT, S17N, and G12D K-Ras mutant expressing cells (Fig. 6*C*, *filled squares*) albeit variation across but not within experiments was high (Fig. 6*C*, individual experiments represented as separate colors of *open squares*). Even though the average number of exosomes secreted per cell, as

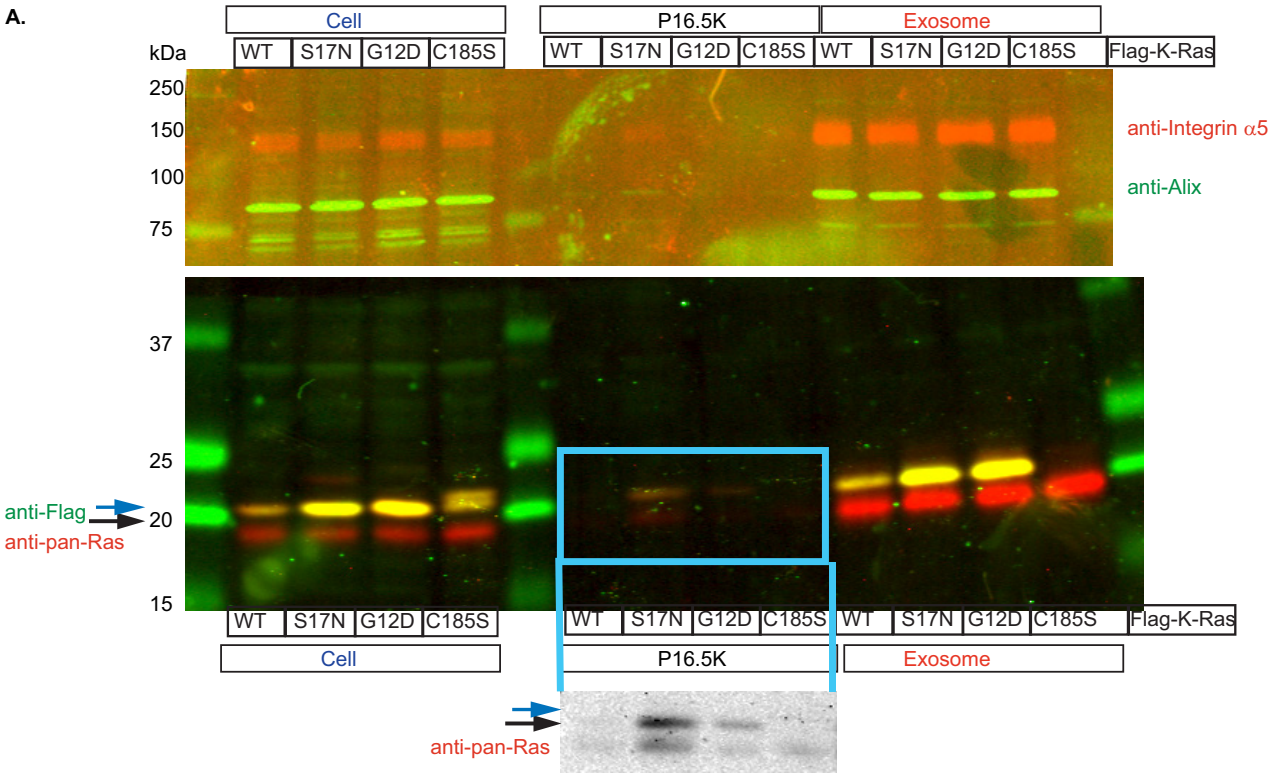
A.
Cell
P16.5K
Exosome
kDa
WT
S17N
G12D
C185S
Flag-K-Ras
250
150
100
75
anti-Integrin α5
anti-Alix
37
25
20
15
anti-Flag
anti-pan-Ras
anti-pan-Ras

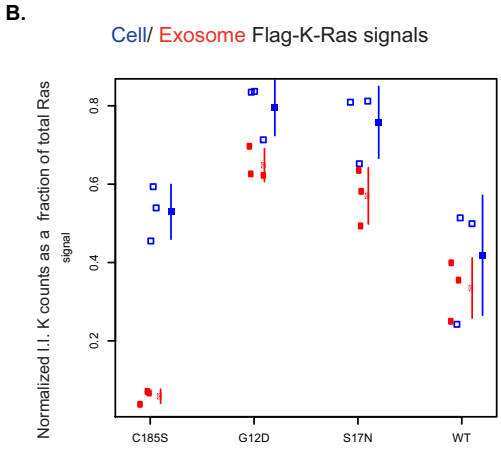
B.
Cell/ Exosome Flag-K-Ras signals
Normalized I.I. K counts as a fraction of total Ras signal
C185S
G12D
S17N
WT

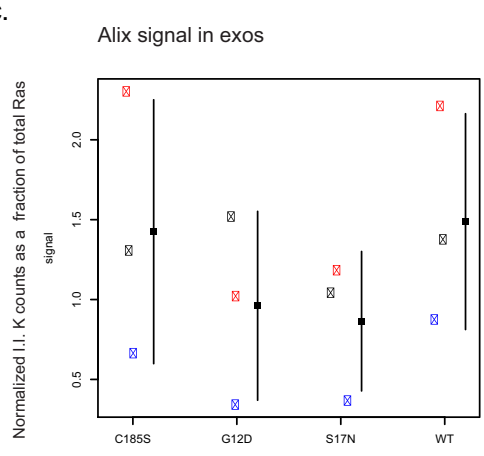
C.
Alix signal in exos
Normalized I.I. K counts as a fraction of total Ras signal
C185S
G12D
S17N
WT

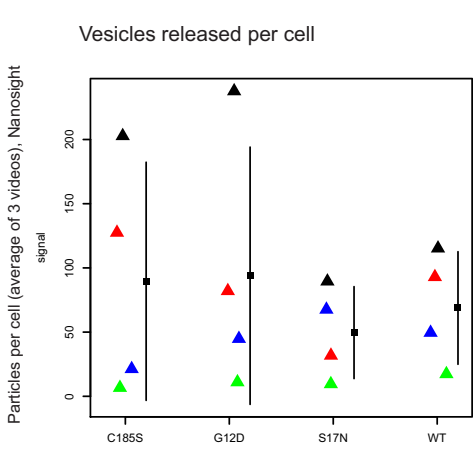
D.
Vesicles released per cell
Particles per cell (average of 3 videos), Nanosight signal
C185S
G12D
S17N
WT

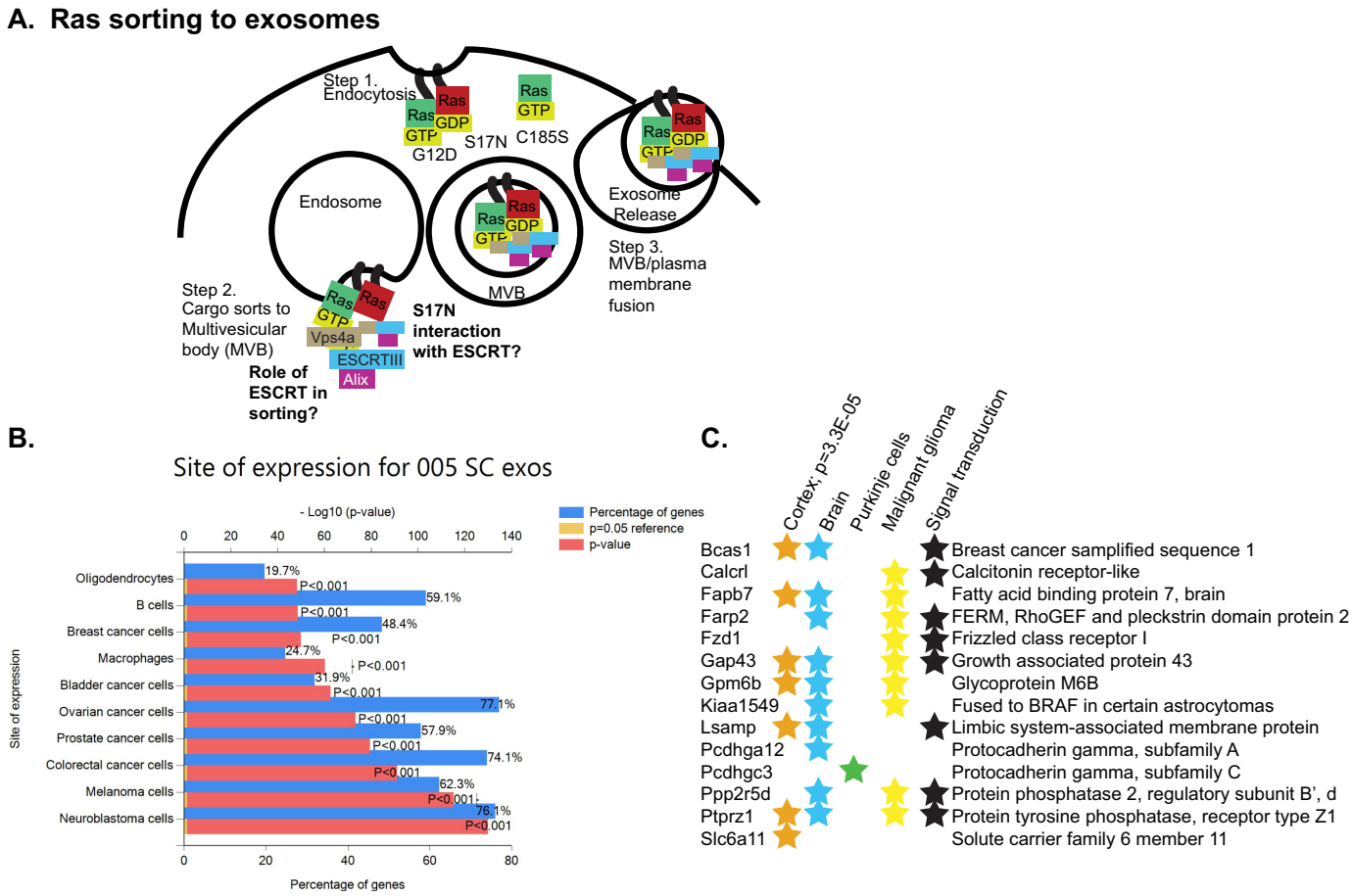

FIGURE 7. **Exosomes have the potential to predict tumor type and signaling at membranes.** *A,* model for Ras sorting to exosomes. *B,* top 10 exosome proteomes (downloaded from ExoCarta for human, mouse, and rat proteomes along with site of expression data) significantly overlapping with 005 exosomes (supplemental Table S4) and compared using the FunRich custom feature. *C,* unique exosome proteins (not represented in ExoCarta) for supplemental Tables S1 and S4 005 exosome proteomic data. Site of expression was mapped using FunRich and the provided database to give the *p* value indicated. *Stars* indicate the presence for each gene symbol (*orange*, cortex; *blue*, brain; *green,* Purkinje cells; *yellow*, malignant glioma; *black*, signal transduction).

predicted by NanoSight NTA, was lowest for cells expressing Flag-K-Ras S17N (Fig. 6*D*), these values were highly variable across experiments (Fig. 6*D*, individual experiments depicted as separate colors of *filled triangles*), with cells expressing the S17N mutant releasing more exosomes per cell than the G12D mutant in one of the 4 independent experiments (Fig. 6*D*, compare *blue filled triangles*). In sum, we concluded that the K-Ras signaling status does not significantly affect the total amount of exosomes released per cell.

Discussion

Herein, we demonstrated that the GBM exosome proteome is enriched for intracellular signaling proteins and Ras protein signal transduction as compared with the whole cell proteome (Fig. 2). Signaling proteins in exosome preparations maintained their topology (Fig. 3), and we were able to detect active Ras in both 005 and U87MG GBM cells, which copurified with ESCRT-associated proteins in GST-Raf-RBD precipitation assays (Fig. 4).

Our studies revealed that K-Ras farnesylation, but not GTP binding, was necessary for K-Ras packaging within exosomes (Fig. 6). The predicted path of Ras proteins to exosomes, based on this study and others (53, 67, 72–76), is modeled in Fig. 7*A*. Ras proteins are sorted to exosomes in a manner dependent upon farnesylation but not GTP binding (step 1). Our studies (Fig. 4) detected ESCRTIII interactors Vps4a and Alix in co-precipitates of active Ras from exosomes lysates, but not another ESCRT substrate, integrin α5 (63). This is consistent with a prior publication

FIGURE 6. **Farnesylation, but not GTP binding, is necessary for K-Ras trafficking to exosomes.** *A,* immunoblot from a single gel cut to blot with multiple indicated antibodies. Samples from U87MG cells stably expressing induced Tet-Flag-K-Ras for attached cells (*cell*), larger vesicles and debris (*P16.5Kxg*), and exosomes were analyzed by loading the cell number normalized equivalents within each group. Cell group contains 31.2-fold less cell equivalents than exosomes and P16.5K group is loaded at 3-fold less cell equivalents than exosomes. *Green font* (700) and *red font* (800) represent Li-Cor Odyssey channels. *Blue arrows*, unfarnesylated Flag-K-Ras; *black arrows*, farnesylated Flag-K-Ras. P16.5K samples are shown as a cutout (indicated by *light blue box/lines*) *below* the complete blot. Cutout image shown in *black and white* at higher intensity while conserving linearity using Odyssey scale adjustment to more readily observe pan-Ras signal showing both FLAG and endogenous Ras (*B* and *C*) Ras (Flag-K-Ras and pan-Ras) and Alix signals on blots were normalized to integrin α5 signal, and a fraction of Flag-K-Ras in total Ras signal (Flag-K-Ras plus pan-Ras) was calculated. Stripcharts for fraction values for 3 independent experiments ((*B*, whole cell, *open blue squares*; exosomes, *closed red squares*; *C,* Alix, *open squares*) were plotted with means as a *symbol* along a segment depicting mean ± S.D. *B,* note: greater amounts of cell equivalents were loaded for exosomes than cells to facilitate analysis without splitting the *y* axis, which is not accounted for on the plot. *D,* number of particles per cell for 4 independent experiments (*filled triangles*) each averaging 3 tracking analyses (*filled squares* along segment) plotted mean ± S.D. (segments). *C* and *D,* independent experiments represented as separate colors of *symbols*.

demonstrating a direct Vps4a and ESCRTIII interaction with Ras proteins (67). These proteins would be expected to function in the intralumenal sorting of Ras to a MVB, although their precise role in Ras sorting and whether they interact with the GTP binding mutant S17N is unclear from this analysis (step 2). Fusion of the MVB with the plasma membrane enables the extracellular release of the intralumenal vesicle carrying Ras, now deemed an exosome (step 3).

Although our model appears to define the requirement for ESCRT and its interaction with Ras in the production of exosomes, this is an area of uncertainty. One might expect from our results that Vps4a would be able to interact equally well with K-Ras S17N and G12D, but we were unfortunately unable to affinity purify enough Flag-K-Ras from exosome lysates to perform co-precipitation experiments. The formation of MVBs by pathways independent of ESCRT has been described (77, 78) and the role of ceramide, a cone-shaped sphingolipid generated by neutral sphingomyelinase activity to promote exosome formation, was not investigated. Moreover, it is possible that Ras-bearing vesicles, perhaps in association with ESCRT proteins, are budding directly from the plasma membrane through a different process. Nevertheless, the K-Ras S17N mutant failed to alter the amount of Alix released from cells and was released to exosomes in similar amounts as K-Ras G12D (Fig. 6). At the very least, these results support a model by which dominant-negative Ras signaling by the S17N mutant does not significantly alter exosome or extracellular vesicle biogenesis.

A lack of requirement for GTP binding in the release of K-Ras to exosomes is not entirely surprising, because a recent study of K-Ras did not find any statistically significant differences between the percentages of G12V and S17N mutants localized to endosomes (79). By contrast, this prior study revealed an increase in the fluorescence recovery after photobleaching half-time and immobile fractions for the GFP K-Ras S17N mutant as compared with GFP fusions to either active forms of K-Ras (wild-type or G12V). Although that would seem to indicate that the amount of exosomes released from cells might be influenced by K-Ras signaling by altering the amounts of exosomes produced or the numbers of proteins trafficking to exosomes, our studies did not detect any significant impact of the GTP binding status upon the number of exosomes or amount of Alix released per cell (Fig. 6).

Our results support the idea that membrane association, rather than random integration of cytoplasmic components within vesicles, dictates the trafficking of proteins to exosomes. First, our data show that greater than 40% of the identified 005 exosome proteome are plasma membrane factors (Fig. 3*D*), which is far greater than that observed for the 005 cellular proteome (less than 16%). Second, translation proteins are less significantly represented in exosomes using sucrose cushion preparation, and the ribosomal protein Rps3 was found to be on the surface of exosomes based upon its lack of protection against trypsin and its lower level of retention in sucrose cushion-purified exosomes (Fig. 3). Third, exosomes distinctly lack unfarnesylated, cytoplasmic K-Ras, demonstrating that it cannot "piggyback" on other proteins and is not randomly integrated from the cytoplasm into vesicles. Overall, these results are consistent with a previous publication showing that highly oligomeric, cytoplasmic proteins can be targeted to exosomes/microvesicles by lipid membrane anchors (80). Thus, one interesting question for future investigation is whether RNA localizing to exosomes might also be incorporated in a membrane localization-dependent manner.

Exosomes are enriched for signaling and cell communication proteins that are carried in their functional orientation (Figs. 2 and 3). Our analysis of Ras signaling revealed that exosomes contain active Ras in complex with ESCRTIII-associated proteins. These data suggest that exosome protein modifications, activity, and interactions could be used to predict the tumor signaling status. Interestingly, exosomes released from both U87MG (derived from a human glioblastoma devoid of Ras mutations (66)) and 005 cells (carrying H-Ras G12V (51)) carried similar levels of active Ras proteins. This suggests that U87MG also relies upon activated Ras signaling, and this is further supported in that U87MG cells treated with a Ras inhibitor exhibit a decrease in HIF-1α causing a reduction in glycolysis gene transcription and cell death (44).

Exosomes present an accessible source of information for understanding tumor type in addition to signaling status. Comparing our data to a compilation of previously published exosome proteomes available at ExoCarta (57–60) demonstrates that many factors are shared across exosome proteomes, yet some are unique. Nearly 94% of the 005 exosome proteins overlapped with proteins logged in the ExoCarta database (Fig. 2*B*). Non-cancer cell type exosome proteomes (B cells, macrophages, and oligodendrocytes) displayed significant overlap with the highly purified 005 mouse glioblastoma exosome proteome (supplemental Table S4), falling within the top 10 of 37 sites of expression analyzed (Fig. 7*B*), when compared with human, mouse, and rat exosome proteomes publicly available at ExoCarta. We speculate that this is due to a large number of proteins regulating exosome dynamics that are shared among all cell types (*e.g.* CD81, ESCRT proteins, etc.). However, the most significant similarity to 005 exosomes was observed for exosomes from another central nervous system tumor, neuroblastoma (Fig. 7*B*), indicating that some of the proteins trafficked to exosomes could predict the tumor type due to tissue specificity.

We also found unique proteins in exosomes that were clearly associated with the tumor site of origin, many of which regulate signal transduction. Because there were no glioblastoma exosomal proteomic data sets available at ExoCarta, we examined unique proteins not represented in ExoCarta but present in 005 exosomes (for supplemental Tables S1 and S4) and classified their site of expression using FunRich (Fig. 7*C*). Interestingly, 9 of these 14 proteins mapped to malignant glioma as their site of expression, and 7 were significantly representative of the cortex ($p = 3.3 \times 10^{-5}$). The remaining proteins were represented within the brain or Purkinje neurons. Of these proteins, 8 function in signal transduction. Taken together, these results suggest that exosomes carry tissue-specific proteins that could indicate tumor site of origin and provide insight into how tumors are signaling.

Current research has already revealed a capacity to identify altered protein, RNA, and DNA expression profiles in exosomes from patients as compared with a control population using exosomes isolated from various bodily fluids (26–31, 81,

TABLE 1
Primers used in cloning and sequencing

Primer name	Sequence 5′ to 3′
oNL42	CAACTAGAAGGCACAACTAGTTATGGCTGATTATGATCTAGAGTCG
oNL71	GAAGGATCCATGGACTACAAGGACGACGATGACAAGTCCGGAACTGAATATAAACTTGTGGTAGTTGGAG
oNL63	GTGGCGTAGGCAAGAATGCATTGACGATACAGCTAATTCAGAATCATTTTGTGGACG
oNL64	GCTGTATCGTCAATGCATTCTTGCCTACGCCACCAGCTCCAACTACC
oNL57	GAAGGATCCATGGACTACAAGGACGACGATGACAAG

82). Thus, as additional data become available for exosome proteomes from multiple tumor types, particularly coupled with information on signaling status, post-translational modifications, DNA, and RNA, molecular signatures might be identified to predict tumor type and signaling status.

Apart from advancing the field of diagnostics, exosome studies could elucidate a mechanism for intercellular signaling, because signaling and communication proteins are abundant in these vesicles and exist in an active and functional orientation. Intercellular transfer of K-Ras G13D has been proposed to contribute to metastasis in colon cancer based on the ability of exogenous exosome treatment to enhance growth of cells in collagen matrix and soft agar (48). GBM tumors rarely metastasize (83), but experiments probing the uptake of GBM exosomes by endothelial cells and the impact upon angiogenesis (6) indicate that transfer of active signals might be involved in this process. However, a direct exosome protein to cytoplasmic acceptor cell protein interaction has yet to be identified to clearly define whether signaling factors within exosomes indeed function in the cytoplasm of the acceptor cell and how this process might work. Future studies are needed to probe whether active Ras released to exosomes is indeed capable of signaling in another cell.

Experimental Procedures

Cell Culture and Stable Cell Line Generation—005 cells (51) were cultured as previously described in N2 medium: DMEM/F-12 supplemented with 1× N2, hEGF (20 ng/ml), hFGF-2 (20 ng/ml), Heparin (40 μg/ml), and L-glutamine to maintain an undifferentiated state. U87MG cells (66) were cultured in DMEM (4.5 g/liter glucose, L-glutamine, and sodium pyruvate) supplemented with 10% FBS. Penicillin/streptomycin (Corning, 1X) and Cipro (10 μg/ml) antibiotics were added to maintain cultures. All cells were cultured at 37 °C in 5% CO_2.

U87MG cells stably expressing lentiviral Tet-Flag-K-Ras expression plasmids were selected as a batch for puromycin resistance using 3 μg/ml of puromycin and validating complete eradication of control cells cultured in parallel. Puromycin selection was continuously applied to cultures to ensure retention of expression constructs, and doxycycline was excluded from passaged cultures and added only for experimental analyses to promote the maintenance of isogenic comparisons of K-Ras mutants.

Cloning of Lentiviral Vectors: Flag-K-Ras Expression Constructs—Primers (Table 1) and plasmids (Table 2) used to clone and validate these constructs are summarized in Tables 1 and 2. We created a single lentiviral vector expressing Flag-K-Ras through a third generation Tet-responsive system (Fig. 5*A*). Between the two long terminal repeats (LTR) of this vector, Flag-K-Ras is expressed under a TRE3GV promoter, and the genes encoding Tet-On 3G (Clontech) transactivator protein and puromycin *N*-acetyltransferase (PuroR) are dually expressed by the EF1a promoter, using the T2A self-cleaving peptide (86) to generate separate proteins, and the woodchuck hepatitis virus posttranscriptional regulatory element in the 3′ untranslated region (UTR) to enhance expression (87).

TABLE 2
Source of plasmids used as templates in PCR

Plasmid No.	Name	Source
pRAR3G	TRE3G PURO	Gift of the Verma lab
	CMV-nLuc -linker-HA-GGA-TCC-K-Ras WT	Gift of the Wahl lab
	CMV-nLuc -linker-HA-GGA-TCC-K-Ras G12D	Gift of the Wahl lab
pLi656	CMV-cLuc-linker-HA-GGA-TCC-K-Ras Y40C	Gift of the Wahl lab
13338	GST-Raf-RBD	Addgene (85)
	CMV-nLuc -linker-HA-GGA-TCC-K-Ras C185S	Gift of the Wahl lab
pNL10	CMV-nLuc -linker-HA-GGA-TCC-K-Ras S17N	This study

To make Flag-K-Ras WT, G12D, and C185S expression constructs, CMV-nLuc-HA-K-Ras given to us by the Wahl lab were PCR amplified using the oNL42 primer used in BiLC subcloning and the oNL71 primer containing the BamHI cut sequence, and ATG, the FLAG sequence, a Ser-Gly linker, and K-Ras priming sequences. BamHI-Flag-Ser-Gly-K-Ras-SpeI digested and purified fragments were ligated to BamHI-SpeI-digested lentiviral backbone. Because a Flag-K-Ras S17N template was not available, we used the shorter plasmid CMV-nLuc-HA-K-Ras WT as a template for site-directed mutagenesis with primers oNL63 and oNL64 to make an accurate template first. Then, the Flag-K-Ras S17N lentiviral Tet expression construct was cloned using the CMV-nLuc-HA-K-Ras S17N template and oNL42 and oNL71 primers as for other Flag-K-Ras expression constructs. To verify the absence of unintended mutations within Flag-K-Ras plasmids, each ORF of the constructs was sequenced in entirety using oNL42 and oNL57 and/or oNL71.

Ultracentrifugation Harvesting of Exosomes—This protocol was adapted from traditional exosome harvesting protocols (12, 54). Cells were grown in their usual medium for 24 h. For Tet induction experiments, the stable Tet analogue Dox was added 3 h prior to the final 3 h of the 24-h incubation to ensure efficient expression of constructs during exosome harvesting. Medium was removed and replaced with fresh exosome-harvesting medium (containing exosome-depleted FBS for cells grown in FBS-supplemented medium and Dox at the indicated concentrations for specified experiments). Exosome depletion of FBS was achieved by centrifuging FBS overnight at 110,000 × *g* to pellet exosomes, and then FBS supernatants were sterile filtered with 0.2-μm doxycycline filters. Cells were grown for 48 h in exosome-harvesting medium, then conditioned

medium was collected from plates and spun at 300 × *g* to remove cells. In parallel, lysates were prepared from cells, and cells from one plate were counted to calculate the total number of exosome-producing cells. Supernatants from the 300 × *g* spin were spun at 16,500 × *g* for 20 min to remove dead cells and cellular debris, and supernatants were then pooled and filtered using 0.2-μm filters to retain only smaller vesicles. Exosomes were harvested from filtered supernatants by spinning at 110,000 × *g* for 1 h and washing pooled samples in PBS. An additional 110,000 × *g* spin for 1 h in a smaller volume of PBS was performed to concentrate the exosomes for experimental analyses.

TEM Analysis of Exosomes—For TEM analyses, ultracentrifugation harvested exosomes were fixed in 4% formaldehyde (EM grade), and these were mounted on grids using methods previously described (54) and observed at ×20,000 magnification on a Zeiss Libra 120 PLUS EF-TEM Transmission Electron Microscope, equipped with a 2kx2k fiber optically coupled bottom mount YAG CCD camera for image acquisition. Using Fiji (ImageJ 1.50a), the diameter of the exosomes (nm) was calculated for 230 exosomes (005) or 262 exosomes (U87MG) from 4 separate images for each after adjusting pixel width and height to 0.7 nm/pixel.

Protein Quantitation—Exosomes were permeabilized for 30 min on ice in 0.1% Triton X-100 prior to quantitation. Cell lysates were diluted 1:5 for analysis. BSA standards were prepared using the appropriate buffer (0.1% Triton X-100 or 20% lysis buffer). DC protein assay (Bio-Rad) reagents and protocol were used, and samples were calculated in parallel to a BSA standard series. All samples were plated in triplicate and averaged on 96-well plates and A_{750} readings were recorded on a TECAN M1000pro.

Sucrose Cushion Purification of Exosomes—For sucrose cushion purification of exosomes, we adapted the following protocol (54). We prepared more than 2.05 mg (by total protein quantification) of ultracentrifugation-harvested exosomes. We reserved 50 μg (25%) of exosomes to compare crude ultracentrifugation purified to further, sucrose cushion-purified exosomes. Using an SW41 tube, 2 mg of ultracentrifugation-harvested exosomes were diluted into 10 ml of PBS, and this was loaded on top of 2 ml of a Tris/D_2O sucrose cushion prepared according to the instructions defined in the Thery protocol (54). Tubes were spun at 110,000 × *g* (25,000 rpm in an SW41 rotor) for 75 min, and 9.2 ml from the top layer was diluted into 20.8 ml of PBS, whereas 1.8 ml from the top of the cushion was diluted into 28.2 ml of PBS. Diluted samples were spun at 110,000 × *g* for 60 min in an SW32 rotor. Pellets from this spin were resuspended into 1 ml of PBS and spun for 60 min in an MLA-150 rotor on a benchtop ultracentrifuge at 110,000 × *g* to further wash and concentrate the pellets.

Mass Spectrometry (MS)—Equal amounts of total protein were compared in MS experiments. The samples were first denatured in 8 M urea and then reduced and alkylated with 10 mM Tris(2-carboxyethyl)phosphine hydrochloride (Roche Applied Science) and 55 mM iodoacetamide (Sigma), respectively. The samples were then digested overnight with trypsin (Promega) according to the manufacturer's specifications. The protein digests were pressure-loaded onto 250-μm inner diameter fused silica capillary (Polymicro Technologies) columns with a Kasil frit packed with 3 cm of 5-μm Partisphere strong cation exchange resin (Whatman) and 3 cm of 5-μm C18 resin (Phenomenex). After desalting, each biphasic column was connected to a 100-μm inner diameter fused silica capillary (Polymicro Technologies) analytical column with a 5-μm pulled-tip, packed with 10 cm of 5-μm C18 resin (Phenomenex).

Each MudPIT column was placed in line with an 1100 quaternary HPLC pump (Agilent Technologies) and the eluted peptides were electrosprayed directly into an LTQ Orbitrap XL mass spectrometer (Thermo Scientific). The buffer solutions used were 5% acetonitrile, 0.1% formic acid (buffer A), 80% acetonitrile, 0.1% formic acid (buffer B) and 500 mM ammonium acetate, 5% acetonitrile, 0.1% formic acid (buffer C). A 12-step MudPIT was run with salt pulses of 0, 10, 20, 30, 40, 50, 60, 70, and 100% buffer C and 90% buffer C, 10% buffer B. The 120-min elution gradient had the following profile: 10% buffer B beginning at 15 min to 40% buffer B at 105 min, continuing to 110 min. A cycle consisted of one full scan mass spectrum (400–1600 m/z) in the Orbitrap at 60,000 resolution followed by five data-dependent collision-induced dissociation MS/MS spectra in the LTQ. Charge state screening was enabled and unassigned charge states and charge state 1 were rejected. Dynamic exclusion was enabled with a repeat count of 1, a repeat duration of 30 s, an exclusion list size of 500, and an exclusion duration of 180 s. Dynamic exclusion early expiration was enabled with an expiration count of 3 and an expiration signal-to-noise ratio of 3. Application of mass spectrometer scan functions and HPLC solvent gradients were controlled by the Xcalibur data system (Thermo Scientific).

MS/MS spectra were extracted using RawXtract (version 1.9.9) (88). MS/MS spectra were searched with the Sequest (version 3.0) algorithm (89) against a mouse international protein index (IPI) database (version 3.30, release date 06-28-2007) supplemented with known contaminants and concatenated to a decoy database in which the sequence for each entry in the original database was reversed (90). A total of 113,149 protein entries were searched. Precursor mass tolerance was 50 ppm and fragment mass tolerance was 600 ppm. For protein identifications, the Sequest search was performed using no enzyme specificity and static modification of cysteine due to carboxyamidomethylation (57.02146). Sequest search results were assembled and filtered using the DTASelect (version 2.0.49) algorithm (91), requiring peptides to be at least half-tryptic (cleavage C-terminal to Arg or Lys residue) and a minimum of two peptides per protein identification. The number of missed cleavages was not specified. The protein identification false-positive rate was kept below 1% and all peptide-spectra matches had less than 10 ppm mass error. DTASelect assesses the validity of peptide-spectra matches using the cross-correlation score (XCorr) and normalized difference in cross-correlation scores (ΔCN). The search results are grouped by charge state and tryptic status and each subgroup is analyzed by discriminate analysis based on a non-parametric fit of the distribution of forward and reversed matches.

Trypsin Protection Assay—Equal volumes of exosomes (7–10 μg of protein) were probed for protection of cytoplasmic proteins by examining treatment with: trypsin (1 μg), trypsin and

TABLE 3
Antibodies used in this study

Protein detected	Source No. (dilution for immunoblots)
pan-Ras	Antibody included with CST Ras detection kit (1:1000) andCST#3965 (1:1000)
Alix	Santa Cruz sc-49268 (1:200)
Calnexin	Santa Cruz sc-11397 (1:200)
β-Catenin	BD Biosciences No. 610153 (1:1000)
Rps3	CST#9538 (1:1000)
GST	Hunter lab affinity purified antibody (1:200)
Vps4a	Sigma, No. SAB4200022 (1:1000)
Integrin α5	CST#4705 (1:1000)
FLAG	Sigma No. F3165 (1:2500)
Tubulin	Sigma No. T5168 (1:8000)
pERK1/2 Thr-202/ Tyr-204	CST#4376 (1:1000)
Hsp60	Santa Cruz sc-1052 (1:1000)
Tsg101	Santa Cruz sc-6037 (1:1000)
Histone H3	Abcam ab1791 (1:5000)

Triton X-100 (0.1%), or control. The purified GST-Ubc9 protein was included at 5 ng/reaction to demonstrate the ability of trypsin to digest a soluble, non-exosomal protein. Digests were incubated for 3 h at 37 °C, and inactivation was achieved by adding protease inhibitors at the following final concentrations: PMSF (5 mM), leupeptin (40 μM), and aprotinin (2.5 μM). We then immediately added protein loading buffer to 1× and boiled samples for 5 min at 95 °C.

Active Ras Purification Assay—This experiment was performed according to the manufacturer's protocol (active Ras precipitation kit, Cell Signaling Technology). Exosomes (18 μg protein) were pelleted at 110,000 × *g* in 1 ml of PBS, and pellets were lysed with the included lysis buffer and 1 mM PMSF added. We added 80 μg of GST-Raf-RBD protein to lysates, then we reserved 10% for analysis of total input prior to active Ras precipitation. Mixtures were incubated with resin for 1 h at 4 °C with rotation. Unbound proteins were pelleted, and 5% of this volume was saved for analysis. Resin with bound proteins were washed three times with the included lysis/binding/wash buffer, and 5% of the first wash was saved for analysis. Bound proteins were eluted and boiled using 50 μl of the included 2× SDS loading buffer with DTT added to 200 mM. Half of the eluate was resolved on a gel next to input, unbound, and wash samples.

Immunoblot Analyses—Antibodies used in this study are summarized in Table 3. Samples were resolved on polyacrylamide gels consisting of a separating gel [12.5% (w/v) acrylamide, 0.1% (w/v) bisacrylamide, 0.38 M Tris-Cl, pH 8.8, 0.1% (w/v) SDS] and a stacking gel [4% (w/v) acrylamide, 0.1% (w/v) bisacrylamide, 0.125 M Tris-Cl, pH 6.8, 0.1% (w/v) SDS] using standard protocols for SDS-PAGE, and gels were transferred overnight at 4 °C with constant voltage (22 V) to PVDF membranes optimized for Odyssey detection. Li-Cor Odyssey protocols were followed for blotting of membranes with primary and secondary antibodies (Alexa dye 680 and IRDye 800), and after washing, these were scanned to the Li-Cor Odyssey for quantitative detection of signals. For quantitation, bands for proteins of interest were manually defined using a rectangle or ellipse, and an identical size/shape background band was manually defined (user defined background method). Normalized intensities were calculated from I.I.K counts given by the Li-Cor Odyssey software by subtracting background values from bands of interest and calculating this signal as a fraction of background-subtracted signal for a normalizing protein.

NanoSight Counting of Exosomes—NanoSight NTA was used to roughly calculate the number of vesicles in an exosome purification. Three videos of 1 min each were captured and averaged for each sample. Experimental analyses were performed on exosomes harvested from cells on 4 separate dates and averaged for presented data.

Data Analysis—For MS experiments, proteins with less than a 1% false-positive rate were identified for each in triplicate using Sequest search and DTASelect filtering from MS/MS spectra. Returned IPI identifiers were analyzed only if these were observed in all three technical replicates, and results were filtered to prevent duplication of identifiers and proteins (by looking at genes predicted by identifier) in the analysis.

Functional analyses of predicted proteomes were performed by loading IPI identifiers from our filtered list to the DAVID version 6.7 functional annotation tool (61, 62), and the functional annotation chart tool, specifically GO_BP_FAT, was used to look for significantly represented gene ontology terms for biological process. Data from the GO_BP_FAT charts were used to create separate lists of significantly represented biological processes for whole cell and exosome proteomes, using a p value of 0.05 or less as the cutoff (supplemental Table S2, GO_BP_FAT_CELL3 and GO_BP_FAT_EXO3, all terms above the underline are p values less than 0.05). To probe for unique terms, we compared significantly represented terms using a tool designed to detect set differences (jura.wi.mit.edu/bioc/tools/compare.php).

The FunRich tool (56) was used for specified analyses. Gene symbols were acquired for IPI IDs using DAVID and the bioDBnet db2db converter (92). The FunRich database was used for mapping sites of expression, cellular component, and biological process except for comparisons to exosome datasets from ExoCarta (57–60), in which a custom spreadsheet for site of expression was generated from Experiment Details (to link information from experiment number to tissue of origin information) and Protein mRNA Details files (sorting in Excel for human, mouse, and rat proteomes results from mass spectrometry analyses).

For data analysis, *R* (R Core Team (2015), R: A language and environment for statistical computing; R Foundation for Statistical Computing, Vienna, Austria) was used to calculate mean, S.D., and generate stripcharts from this data.

Author Contributions—N. L. conceived and designed the experiments, performed data acquisition, analysis and interpretation, drafted the article, and participated in final approval of the article for publication. T. H. contributed to the design of the experiments, interpretation of data, revision of the article, and participated in final approval of the article for publication. A. A. designed, acquired data, and advised in analysis/interpretation of MudPIT/MS experiments, edited sections referring to MS, and participated in final approval of the article for publication. J. R. Y. participated in the design of the MudPIT/MS technology, critical analysis of manuscript, and participated in final approval of the article for publication.

Acknowledgments—We thank Dr. Inder Verma and members of his laboratory, particularly Dr. Amy Rommel, for providing all cell lines established from mouse tumors, the lentiviral vector (pRAR3G) used for cloning, and valuable advice on cell culture, lentiviral cloning, and transduction. We are grateful for the generous gift of plasmids containing sequences for cloning K-Ras from Dr. Yao-Cheng Li (Dr. Geoff Wahl's lab) and for expert advice and recommendations regarding Ras studies. We express our appreciation for the work of Dr. Sarah Dunn and Matt Joens of the Waitt Advanced Biophotonics Core in TEM imaging and for providing guidance in the analysis of results. We also thank Dr. Walter Eckhart and all members of the Hunter laboratory for feedback on this project and the development of this manuscript.

References

1. Schneider, A., and Simons, M. (2013) Exosomes: vesicular carriers for intercellular communication in neurodegenerative disorders. *Cell Tissue Res.* **352,** 33–47
2. Robbins, P. D., and Morelli, A. E. (2014) Regulation of immune responses by extracellular vesicles. *Nat. Rev. Immunol.* **14,** 195–208
3. Grange, C., Tapparo, M., Collino, F., Vitillo, L., Damasco, C., Deregibus, M. C., Tetta, C., Bussolati, B., and Camussi, G. (2011) Microvesicles released from human renal cancer stem cells stimulate angiogenesis and formation of lung premetastatic niche. *Cancer Res.* **71,** 5346–5356
4. Hong, B. S., Cho, J. H., Kim, H., Choi, E. J., Rho, S., Kim, J., Kim, J. H., Choi, D. S., Kim, Y. K., Hwang, D., and Gho, Y. S. (2009) Colorectal cancer cell-derived microvesicles are enriched in cell cycle-related mRNAs that promote proliferation of endothelial cells. *BMC Genomics* **10,** 556
5. Hood, J. L., Pan, H., Lanza, G. M., and Wickline, S. A., Consortium for Translational Research in Advanced Imaging and Nanomedicine (C-TRAIN)). (2009) Paracrine induction of endothelium by tumor exosomes. *Lab. Investig.* **89,** 1317–1328
6. Kucharzewska, P., Christianson, H. C., Welch, J. E., Svensson, K. J., Fredlund, E., Ringnér, M., Mörgelin, M., Bourseau-Guilmain, E., Bengzon, J., and Belting, M. (2013) Exosomes reflect the hypoxic status of glioma cells and mediate hypoxia-dependent activation of vascular cells during tumor development. *Proc. Natl. Acad. Sci. U.S.A.* **110,** 7312–7317
7. Mineo, M., Garfield, S. H., Taverna, S., Flugy, A., De Leo, G., Alessandro, R., and Kohn, E. C. (2012) Exosomes released by K562 chronic myeloid leukemia cells promote angiogenesis in a Src-dependent fashion. *Angiogenesis* **15,** 33–45
8. Nazarenko, I., Rana, S., Baumann, A., McAlear, J., Hellwig, A., Trendelenburg, M., Lochnit, G., Preissner, K. T., and Zöller, M. (2010) Cell surface tetraspanin Tspan8 contributes to molecular pathways of exosome-induced endothelial cell activation. *Cancer Res.* **70,** 1668–1678
9. Park, J. E., Tan, H. S., Datta, A., Lai, R. C., Zhang, H., Meng, W., Lim, S. K., and Sze, S. K. (2010) Hypoxic tumor cell modulates its microenvironment to enhance angiogenic and metastatic potential by secretion of proteins and exosomes. *Mol. Cell. Proteomics* **9,** 1085–1099
10. Salomon, C., Ryan, J., Sobrevia, L., Kobayashi, M., Ashman, K., Mitchell, M., and Rice, G. E. (2013) Exosomal signaling during hypoxia mediates microvascular endothelial cell migration and vasculogenesis. *PloS One* **8,** e68451
11. Sharghi-Namini, S., Tan, E., Ong, L. L., Ge, R., and Asada, H. H. (2014) Dll4-containing exosomes induce capillary sprout retraction in a 3D microenvironment. *Sci. Rep.* **4,** 4031
12. Skog, J., Würdinger, T., van Rijn, S., Meijer, D. H., Gainche, L., Sena-Esteves, M., Curry, W. T., Jr., Carter, B. S., Krichevsky, A. M., and Breakefield, X. O. (2008) Glioblastoma microvesicles transport RNA and proteins that promote tumour growth and provide diagnostic biomarkers. *Nat. Cell Biol.* **10,** 1470–1476
13. Tadokoro, H., Umezu, T., Ohyashiki, K., Hirano, T., and Ohyashiki, J. H. (2013) Exosomes derived from hypoxic leukemia cells enhance tube formation in endothelial cells. *J. Biol. Chem.* **288,** 34343–34351
14. Taverna, S., Flugy, A., Saieva, L., Kohn, E. C., Santoro, A., Meraviglia, S., De Leo, G., and Alessandro, R. (2012) Role of exosomes released by chronic myelogenous leukemia cells in angiogenesis. *Int. J. Cancer* **130,** 2033–2043
15. Zhang, L., Wu, X., Luo, C., Chen, X., Yang, L., Tao, J., and Shi, J. (2013) The 786-0 renal cancer cell-derived exosomes promote angiogenesis by down-regulating the expression of hepatocyte cell adhesion molecule. *Mol. Med. Rep.* **8,** 272–276
16. Luga, V., and Wrana, J. L. (2013) Tumor-stroma interaction: Revealing fibroblast-secreted exosomes as potent regulators of Wnt-planar cell polarity signaling in cancer metastasis. *Cancer Res.* **73,** 6843–6847
17. Luga, V., Zhang, L., Viloria-Petit, A. M., Ogunjimi, A. A., Inanlou, M. R., Chiu, E., Buchanan, M., Hosein, A. N., Basik, M., and Wrana, J. L. (2012) Exosomes mediate stromal mobilization of autocrine Wnt-PCP signaling in breast cancer cell migration. *Cell* **151,** 1542–1556
18. Cai, Z., Yang, F., Yu, L., Yu, Z., Jiang, L., Wang, Q., Yang, Y., Wang, L., Cao, X., and Wang, J. (2012) Activated T cell exosomes promote tumor invasion via Fas signaling pathway. *J. Immunol.* **188,** 5954–5961
19. Costa-Silva, B., Aiello, N. M., Ocean, A. J., Singh, S., Zhang, H., Thakur, B. K., Becker, A., Hoshino, A., Mark, M. T., Molina, H., Xiang, J., Zhang, T., Theilen, T. M., Garcia-Santos, G., Williams, C., *et al.* (2015) Pancreatic cancer exosomes initiate pre-metastatic niche formation in the liver. *Nat. Cell Biol.* **17,** 816–826
20. Hood, J. L., San, R. S., and Wickline, S. A. (2011) Exosomes released by melanoma cells prepare sentinel lymph nodes for tumor metastasis. *Cancer Res.* **71,** 3792–3801
21. Hoshino, A., Costa-Silva, B., Shen, T. L., Rodrigues, G., Hashimoto, A., Tesic Mark, M., Molina, H., Kohsaka, S., Di Giannatale, A., Ceder, S., Singh, S., Williams, C., Soplop, N., Uryu, K., Pharmer, L., *et al.* (2015) Tumour exosome integrins determine organotropic metastasis. *Nature* **527,** 329–335
22. Peinado, H., Alečković, M., Lavotshkin, S., Matei, I., Costa-Silva, B., Moreno-Bueno, G., Hergueta-Redondo, M., Williams, C., García-Santos, G., Ghajar, C., Nitadori-Hoshino, A., Hoffman, C., Badal, K., Garcia, B. A., Callahan, M. K., *et al.* (2012) Melanoma exosomes educate bone marrow progenitor cells toward a pro-metastatic phenotype through MET. *Nat. Med.* **18,** 883–891
23. Rodríguez, M., Silva, J., Herrera, A., Herrera, M., Peña, C., Martín, P., Gil-Calderón, B., Larriba, M. J., Coronado, M. J., Soldevilla, B., Turrión, V. S., Provencio, M., Sánchez, A., Bonilla, F., and García-Barberán, V. (2015) Exosomes enriched in stemness/metastatic-related mRNAS promote oncogenic potential in breast cancer. *Oncotarget* **6,** 40575–40587
24. Suetsugu, A., Honma, K., Saji, S., Moriwaki, H., Ochiya, T., and Hoffman, R. M. (2013) Imaging exosome transfer from breast cancer cells to stroma at metastatic sites in orthotopic nude-mouse models. *Adv. Drug Deliv. Rev.* **65,** 383–390
25. Zhang, L., Zhang, S., Yao, J., Lowery, F. J., Zhang, Q., Huang, W. C., Li, P., Li, M., Wang, X., Zhang, C., Wang, H., Ellis, K., Cheerathodi, M., McCarty, J. H., Palmieri, D., *et al.* (2015) Microenvironment-induced PTEN loss by exosomal microRNA primes brain metastasis outgrowth. *Nature* **527,** 100–104
26. Goetzl, E. J., Boxer, A., Schwartz, J. B., Abner, E. L., Petersen, R. C., Miller, B. L., Carlson, O. D., Mustapic, M., and Kapogiannis, D. (2015) Low neural exosomal levels of cellular survival factors in Alzheimer's disease. *Ann. Clin. Transl. Neurol.* **2,** 769–773
27. Gui, Y., Liu, H., Zhang, L., Lv, W., and Hu, X. (2015) Altered microRNA profiles in cerebrospinal fluid exosome in Parkinson disease and Alzheimer disease. *Oncotarget* **6,** 37043–37053
28. Keller, S., Ridinger, J., Rupp, A. K., Janssen, J. W., and Altevogt, P. (2011) Body fluid derived exosomes as a novel template for clinical diagnostics. *J. Transl. Med.* **9,** 86
29. Lugli, G., Cohen, A. M., Bennett, D. A., Shah, R. C., Fields, C. J., Hernandez, A. G., and Smalheiser, N. R. (2015) Plasma exosomal miRNAs in persons with and without Alzheimer disease: altered expression and prospects for biomarkers. *PloS One* **10,** e0139233
30. Melo, S. A., Luecke, L. B., Kahlert, C., Fernandez, A. F., Gammon, S. T., Kaye, J., LeBleu, V. S., Mittendorf, E. A., Weitz, J., Rahbari, N., Reissfelder, C., Pilarsky, C., Fraga, M. F., Piwnica-Worms, D., and Kalluri, R. (2015)

Glypican-1 identifies cancer exosomes and detects early pancreatic cancer. *Nature* **523,** 177–182
31. Tomlinson, P. R., Zheng, Y., Fischer, R., Heidasch, R., Gardiner, C., Evetts, S., Hu, M., Wade-Martins, R., Turner, M. R., Morris, J., Talbot, K., Kessler, B. M., and Tofaris, G. K. (2015) Identification of distinct circulating exosomes in Parkinson's disease. *Ann. Clin. Transl. Neurol.* **2,** 353–361
32. Holmen, S. L., and Williams, B. O. (2005) Essential role for Ras signaling in glioblastoma maintenance. *Cancer Res.* **65,** 8250–8255
33. Friedmann-Morvinski, D., Bushong, E. A., Ke, E., Soda, Y., Marumoto, T., Singer, O., Ellisman, M. H., and Verma, I. M. (2012) Dedifferentiation of neurons and astrocytes by oncogenes can induce gliomas in mice. *Science* **338,** 1080–1084
34. Reilly, K. M., Loisel, D. A., Bronson, R. T., McLaughlin, M. E., and Jacks, T. (2000) Nf1;Trp53 mutant mice develop glioblastoma with evidence of strain-specific effects. *Nat. Genet.* **26,** 109–113
35. McGillicuddy, L. T., Fromm, J. A., Hollstein, P. E., Kubek, S., Beroukhim, R., De Raedt, T., Johnson, B. W., Williams, S. M., Nghiemphu, P., Liau, L. M., Cloughesy, T. F., Mischel, P. S., Parret, A., Seiler, J., Moldenhauer, G., *et al.* (2009) Proteasomal and genetic inactivation of the NF1 tumor suppressor in gliomagenesis. *Cancer Cell* **16,** 44–54
36. Courtois-Cox, S., Genther Williams, S. M., Reczek, E. E., Johnson, B. W., McGillicuddy, L. T., Johannessen, C. M., Hollstein, P. E., MacCollin, M., and Cichowski, K. (2006) A negative feedback signaling network underlies oncogene-induced senescence. *Cancer Cell* **10,** 459–472
37. Schiebe, M., Ohneseit, P., Hoffmann, W., Meyermann, R., Rodemann, H. P., and Bamberg, M. (2000) Analysis of mdm2 and p53 gene alterations in glioblastomas and its correlation with clinical factors. *J. Neurooncol.* **49,** 197–203
38. Jeuken, J., van den Broecke, C., Gijsen, S., Boots-Sprenger, S., and Wesseling, P. (2007) RAS/RAF pathway activation in gliomas: the result of copy number gains rather than activating mutations. *Acta Neuropathol.* **114,** 121–133
39. Prigent, S. A., Nagane, M., Lin, H., Huvar, I., Boss, G. R., Feramisco, J. R., Cavenee, W. K., and Huang, H. S. (1996) Enhanced tumorigenic behavior of glioblastoma cells expressing a truncated epidermal growth factor receptor is mediated through the Ras-Shc-Grb2 pathway. *J. Biol. Chem.* **271,** 25639–25645
40. Verhaak, R. G., Hoadley, K. A., Purdom, E., Wang, V., Qi, Y., Wilkerson, M. D., Miller, C. R., Ding, L., Golub, T., Mesirov, J. P., Alexe, G., Lawrence, M., O'Kelly, M., Tamayo, P., Weir, B. A., *et al.* (2010) Integrated genomic analysis identifies clinically relevant subtypes of glioblastoma characterized by abnormalities in PDGFRA, IDH1, EGFR, and NF1. *Cancer Cell* **17,** 98–110
41. Westermark, B., Heldin, C. H., and Nistér, M. (1995) Platelet-derived growth factor in human glioma. *Glia* **15,** 257–263
42. Adjei, A. A., Davis, J. N., Bruzek, L. M., Erlichman, C., and Kaufmann, S. H. (2001) Synergy of the protein farnesyltransferase inhibitor SCH66336 and cisplatin in human cancer cell lines. *Clin. Cancer Res.* **7,** 1438–1445
43. Amos, S., Redpath, G. T., Polar, G., McPheson, R., Schiff, D., and Hussaini, I. M. (2006) Farnesylthiosalicylic acid induces caspase activation and apoptosis in glioblastoma cells. *Cell Death Differ.* **13,** 642–651
44. Blum, R., Jacob-Hirsch, J., Amariglio, N., Rechavi, G., and Kloog, Y. (2005) Ras inhibition in glioblastoma down-regulates hypoxia-inducible factor-1α, causing glycolysis shutdown and cell death. *Cancer Res.* **65,** 999–1006
45. Bouterfa, H. L., Sattelmeyer, V., Czub, S., Vordermark, D., Roosen, K., and Tonn, J. C. (2000) Inhibition of Ras farnesylation by lovastatin leads to downregulation of proliferation and migration in primary cultured human glioblastoma cells. *Anticancer Res.* **20,** 2761–2771
46. Goldberg, L., and Kloog, Y. (2006) A Ras inhibitor tilts the balance between Rac and Rho and blocks phosphatidylinositol 3-kinase-dependent glioblastoma cell migration. *Cancer Res.* **66,** 11709–11717
47. Russell, J. S., Lang, F. F., Huet, T., Janicot, M., Chada, S., Wilson, D. R., and Tofilon, P. J. (1999) Radiosensitization of human tumor cell lines induced by the adenovirus-mediated expression of an anti-Ras single-chain antibody fragment. *Cancer Res.* **59,** 5239–5244
48. Demory Beckler, M., Higginbotham, J. N., Franklin, J. L., Ham, A. J., Halvey, P. J., Imasuen, I. E., Whitwell, C., Li, M., Liebler, D. C., and Coffey, R. J. (2013) Proteomic analysis of exosomes from mutant KRAS colon cancer cells identifies intercellular transfer of mutant KRAS. *Mol. Cell. Proteomics* **12,** 343–355
49. Subra, C., Grand, D., Laulagnier, K., Stella, A., Lambeau, G., Paillasse, M., De Medina, P., Monsarrat, B., Perret, B., Silvente-Poirot, S., Poirot, M., and Record, M. (2010) Exosomes account for vesicle-mediated transcellular transport of activatable phospholipases and prostaglandins. *J. Lipid Res.* **51,** 2105–2120
50. Tauro, B. J., Mathias, R. A., Greening, D. W., Gopal, S. K., Ji, H., Kapp, E. A., Coleman, B. M., Hill, A. F., Kusebauch, U., Hallows, J. L., Shteynberg, D., Moritz, R. L., Zhu, H. J., and Simpson, R. J. (2013) Oncogenic H-ras reprograms Madin-Darby canine kidney (MDCK) cell-derived exosomal proteins following epithelial-mesenchymal transition. *Mol. Cell. Proteomics* **12,** 2148–2159
51. Marumoto, T., Tashiro, A., Friedmann-Morvinski, D., Scadeng, M., Soda, Y., Gage, F. H., and Verma, I. M. (2009) Development of a novel mouse glioma model using lentiviral vectors. *Nat. Med.* **15,** 110–116
52. Washburn, M. P., Wolters, D., and Yates, J. R., 3rd. (2001) Large-scale analysis of the yeast proteome by multidimensional protein identification technology. *Nat. Biotechnol.* **19,** 242–247
53. Bissig, C., and Gruenberg, J. (2014) ALIX and the multivesicular endosome: ALIX in Wonderland. *Trends Cell Biol.* **24,** 19–25
54. Thery, C., Amigorena, S., Raposo, G., and Clayton, A. (2006) Isolation and characterization of exosomes from cell culture supernatants and biological fluids. *Current Protocols in Cell Biology* (Bonifacino, J. S., ed) Chapter 3, Unit 3 22
55. Svensson, K. J., Christianson, H. C., Wittrup, A., Bourseau-Guilmain, E., Lindqvist, E., Svensson, L. M., Mörgelin, M., and Belting, M. (2013) Exosome uptake depends on ERK1/2-heat shock protein 27 signaling and lipid Raft-mediated endocytosis negatively regulated by caveolin-1. *J. Biol. Chem.* **288,** 17713–17724
56. Pathan, M., Keerthikumar, S., Ang, C. S., Gangoda, L., Quek, C. Y., Williamson, N. A., Mouradov, D., Sieber, O. M., Simpson, R. J., Salim, A., Bacic, A., Hill, A. F., Stroud, D. A., Ryan, M. T., Agbinya, J. I., *et al.* (2015) FunRich: An open access stand alone functional enrichment and interaction network analysis tool. *Proteomics* **15,** 2597–2601
57. Keerthikumar, S., Chisanga, D., Ariyaratne, D., Al Saffar, H., Anand, S., Zhao, K., Samuel, M., Pathan, M., Jois, M., Chilamkurti, N., Gangoda, L., and Mathivanan, S. (2016) ExoCarta: a web-based compendium of exosomal cargo. *J. Mol. Biol.* **428,** 688–692
58. Mathivanan, S., Fahner, C. J., Reid, G. E., and Simpson, R. J. (2012) ExoCarta 2012: database of exosomal proteins, RNA and lipids. *Nucleic Acids Res.* **40,** D1241–1244
59. Mathivanan, S., and Simpson, R. J. (2009) ExoCarta: a compendium of exosomal proteins and RNA. *Proteomics* **9,** 4997–5000
60. Simpson, R. J., Kalra, H., and Mathivanan, S. (2012) ExoCarta as a resource for exosomal research. *J. Extracell. Vesicles* **1,** 10.3402/jev.v1i0.18374
61. Huang da, W., Sherman, B. T., and Lempicki, R. A. (2009) Systematic and integrative analysis of large gene lists using DAVID bioinformatics resources. *Nat. Protocols* **4,** 44–57
62. Huang da, W., Sherman, B. T., and Lempicki, R. A. (2009) Bioinformatics enrichment tools: paths toward the comprehensive functional analysis of large gene lists. *Nucleic Acids Res.* **37,** 1–13
63. Lobert, V. H., Brech, A., Pedersen, N. M., Wesche, J., Oppelt, A., Malerød, L., and Stenmark, H. (2010) Ubiquitination of α5β1 integrin controls fibroblast migration through lysosomal degradation of fibronectin-integrin complexes. *Dev. Cell* **19,** 148–159
64. Zybailov, B., Mosley, A. L., Sardiu, M. E., Coleman, M. K., Florens, L., and Washburn, M. P. (2006) Statistical analysis of membrane proteome expression changes in *Saccharomyces cerevisiae*. *J. Proteome Res.* **5,** 2339–2347
65. Kiel, C., Filchtinski, D., Spoerner, M., Schreiber, G., Kalbitzer, H. R., and Herrmann, C. (2009) Improved binding of raf to Ras.GDP is correlated with biological activity. *J. Biol. Chem.* **284,** 31893–31902
66. Clark, M. J., Homer, N., O'Connor, B. D., Chen, Z., Eskin, A., Lee, H., Merriman, B., and Nelson, S. F. (2010) U87MG decoded: the genomic sequence of a cytogenetically aberrant human cancer cell line. *PLoS Genet.* **6,** e1000832

67. Zheng, Z. Y., Cheng, C. M., Fu, X. R., Chen, L. Y., Xu, L., Terrillon, S., Wong, S. T., Bar-Sagi, D., Songyang, Z., and Chang, E. C. (2012) CHMP6 and VPS4A mediate the recycling of Ras to the plasma membrane to promote growth factor signaling. *Oncogene* **31,** 4630–4638
68. Ostrem, J. M., Peters, U., Sos, M. L., Wells, J. A., and Shokat, K. M. (2013) K-Ras(G12C) inhibitors allosterically control GTP affinity and effector interactions. *Nature* **503,** 548–551
69. Fiordalisi, J. J., Holly, S. P., Johnson, R. L., 2nd, Parise, L. V., and Cox, A. D. (2002) A distinct class of dominant negative Ras mutants: cytosolic GTP-bound Ras effector domain mutants that inhibit Ras signaling and transformation and enhance cell adhesion. *J. Biol. Chem.* **277,** 10813–10823
70. Nassar, N., Singh, K., and Garcia-Diaz, M. (2010) Structure of the dominant negative S17N mutant of Ras. *Biochemistry* **49,** 1970–1974
71. Butch, E. R., and Guan, K. L. (1996) Characterization of ERK1 activation site mutants and the effect on recognition by MEK1 and MEK2. *J. Biol. Chem.* **271,** 4230–4235
72. Baietti, M. F., Zhang, Z., Mortier, E., Melchior, A., Degeest, G., Geeraerts, A., Ivarsson, Y., Depoortere, F., Coomans, C., Vermeiren, E., Zimmermann, P., and David, G. (2012) Syndecan-syntenin-ALIX regulates the biogenesis of exosomes. *Nat. Cell Biol.* **14,** 677–685
73. Baumgärtel, V., Ivanchenko, S., Dupont, A., Sergeev, M., Wiseman, P. W., Kräusslich, H. G., Bräuchle, C., Müller, B., and Lamb, D. C. (2011) Live-cell visualization of dynamics of HIV budding site interactions with an ESCRT component. *Nat. Cell Biol.* **13,** 469–474
74. Bleck, M., Itano, M. S., Johnson, D. S., Thomas, V. K., North, A. J., Bieniasz, P. D., and Simon, S. M. (2014) Temporal and spatial organization of ESCRT protein recruitment during HIV-1 budding. *Proc. Natl. Acad. Sci. U.S.A.* **111,** 12211–12216
75. McCullough, J., Fisher, R. D., Whitby, F. G., Sundquist, W. I., and Hill, C. P. (2008) ALIX-CHMP4 interactions in the human ESCRT pathway. *Proc. Natl. Acad. Sci. U.S.A.* **105,** 7687–7691
76. Scott, A., Gaspar, J., Stuchell-Brereton, M. D., Alam, S. L., Skalicky, J. J., and Sundquist, W. I. (2005) Structure and ESCRT-III protein interactions of the MIT domain of human VPS4A. *Proc. Natl. Acad. Sci. U.S.A.* **102,** 13813–13818
77. Stuffers, S., Sem Wegner, C., Stenmark, H., and Brech, A. (2009) Multivesicular endosome biogenesis in the absence of ESCRTs. *Traffic* **10,** 925–937
78. Trajkovic, K., Hsu, C., Chiantia, S., Rajendran, L., Wenzel, D., Wieland, F., Schwille, P., Brügger, B., and Simons, M. (2008) Ceramide triggers budding of exosome vesicles into multivesicular endosomes. *Science* **319,** 1244–1247
79. Gelabert-Baldrich, M., Soriano-Castell, D., Calvo, M., Lu, A., Viña-Vilaseca, A., Rentero, C., Pol, A., Grinstein, S., Enrich, C., and Tebar, F. (2014) Dynamics of KRas on endosomes: involvement of acidic phospholipids in its association. *FASEB J.* **28,** 3023–3037
80. Shen, B., Wu, N., Yang, J. M., and Gould, S. J. (2011) Protein targeting to exosomes/microvesicles by plasma membrane anchors. *J. Biol. Chem.* **286,** 14383–14395
81. Thakur, B. K., Zhang, H., Becker, A., Matei, I., Huang, Y., Costa-Silva, B., Zheng, Y., Hoshino, A., Brazier, H., Xiang, J., Williams, C., Rodriguez-Barrueco, R., Silva, J. M., Zhang, W., Hearn, S., *et al.* (2014) Double-stranded DNA in exosomes: a novel biomarker in cancer detection. *Cell Res.* **24,** 766–769
82. Kahlert, C., Melo, S. A., Protopopov, A., Tang, J., Seth, S., Koch, M., Zhang, J., Weitz, J., Chin, L., Futreal, A., and Kalluri, R. (2014) Identification of double-stranded genomic DNA spanning all chromosomes with mutated KRAS and p53 DNA in the serum exosomes of patients with pancreatic cancer. *J. Biol. Chem.* **289,** 3869–3875
83. Robert, M., and Wastie, M. (2008) Glioblastoma multiforme: a rare manifestation of extensive liver and bone metastases. *Biomed. Imaging Interv. J.* **4,** e3
84. Li, Y. C., Rodewald, L. W., Hoppmann, C., Wong, E. T., Lebreton, S., Safar, P., Patek, M., Wang, L., Wertman, K. F., and Wahl, G. M. (2014) A versatile platform to analyze low-affinity and transient protein-protein interactions in living cells in real time. *Cell Rep.* **9,** 1946–1958
85. Brtva, T. R., Drugan, J. K., Ghosh, S., Terrell, R. S., Campbell-Burk, S., Bell, R. M., and Der, C. J. (1995) Two distinct Raf domains mediate interaction with Ras. *J. Biol. Chem.* **270,** 9809–9812
86. Hurh, S., Cho, B., You, D. J., Kim, H., Lee, E. M., Lee, S. H., Park, S. J., Park, H. C., Koo, O. J., Yang, J., Oh, K. H., Lee, B. C., Hwang, J. I., and Ahn, C. (2013) Expression analysis of combinatorial genes using a bi-cistronic T2A expression system in porcine fibroblasts. *PloS One* **8,** e70486
87. Donello, J. E., Loeb, J. E., and Hope, T. J. (1998) Woodchuck hepatitis virus contains a tripartite posttranscriptional regulatory element. *J. Virol.* **72,** 5085–5092
88. McDonald, W. H., Tabb, D. L., Sadygov, R. G., MacCoss, M. J., Venable, J., Graumann, J., Johnson, J. R., Cociorva, D., and Yates, J. R., 3rd. (2004) MS1, MS2, and SQT-three unified, compact, and easily parsed file formats for the storage of shotgun proteomic spectra and identifications. *Rapid Commun. Mass Spectrom.* **18,** 2162–2168
89. Eng, J. K., McCormack, A. L., and Yates, J. R. (1994) An approach to correlate tandem mass spectral data of peptides with amino acid sequences in a protein database. *J. Am. Soc. Mass Spectrom.* **5,** 976–989
90. Peng, J., Elias, J. E., Thoreen, C. C., Licklider, L. J., and Gygi, S. P. (2003) Evaluation of multidimensional chromatography coupled with tandem mass spectrometry (LC/LC-MS/MS) for large-scale protein analysis: the yeast proteome. *J. Proteome Res.* **2,** 43–50
91. Tabb, D. L., McDonald, W. H., and Yates, J. R., 3rd. (2002) DTASelect and Contrast: tools for assembling and comparing protein identifications from shotgun proteomics. *J. Proteome Res.* **1,** 21–26
92. Mudunuri, U., Che, A., Yi, M., and Stephens, R. M. (2009) bioDBnet: the biological database network. *Bioinformatics* **25,** 555–556